

Copyright

by

Chukwuemeka I. Okoye

2005

**Carbon Dioxide Solubility and Absorption Rate in
Monoethanolamine/Piperazine/H₂O**

Supervising Committee:

Gary Rochelle, Supervisor

Nicholas A. Peppas

**Carbon Dioxide Solubility and Absorption Rate in
Monoethanolamine/Piperazine/H₂O**

by

Chukwuemeka I. Okoye, B.S.

Thesis

Presented to the Faculty of the Graduate School of
the University of Texas at Austin
in Partial Fulfillment
of the Requirements
for the Degree of

Master of Science in Engineering

The University of Texas at Austin

August, 2005

To My Family

Acknowledgments

I would like sincerely thank Prof. Gary Rochelle for giving me an opportunity to study with him. Dr. Rochelle showed great interest in my development as a researcher and I learned a lot from our numerous weekly meetings. He encouraged questions and always tried to inspire independent thought. I would also like to thank him for affording me the opportunity to participate in a research conference in Vancouver, British Columbia. I enjoyed the opportunity to interact with undergraduate students while serving as a teaching assistant for Senior Plant Design, a course which he taught in the Spring of 2005.

I am also extremely grateful for the financial support provided to me by the Separations Research Program, the U.S. Department of Energy and various other industrial sponsors.

I would like to acknowledge all members of the Rochelle Research group during my stay at UT. It was a pleasure working and interacting with everyone because I developed both professionally and personally. I would like to acknowledge Tunde Oyekan for all the technical and “big picture” discussions we had and the numerous laughs we shared. I would like to acknowledge John McLees and Andrew Sexton for bringing a fresh energy to the group; Tim Cullinane and George Goff for being open, most of the time, to answering any questions I had and Marcus Hilliard for just being himself. Finally, I would like to recognize Ross Dugas and Jennifer Lu for the times we brainstormed together on homework problems and their general camaraderie.

I would also like to thank Jody Lester for her warmth as a person and her willingness to help. Jody was a great facilitator.

I enjoyed taking Mass Transfer taught by Prof. Nicholas Peppas and Separation Technologies taught by Prof. Bruce Eldridge. Those classes provided some of the background for my research and continue to be useful to me today. I would also like to acknowledge Prof. Buddie Mullins for taking interest in my progress and development at UT. Professor Ben Shoulders from the UT Department of Chemistry was also quite helpful with the NMR measurements.

Finally, I am also eternally grateful to my parents for instilling in me great values and a positive outlook on life. These have allowed me to navigate my life thus far in a manner that I am proud of and very thankful to God for.

**Carbon Dioxide Solubility and Absorption Rate in
Monoethanolamine/Piperazine/H₂O**

Publication No. _____

Chukwuemeka I. Okoye, M.S.E.

The University of Texas at Austin, 2005

Supervisor: Gary T. Rochelle

The solubility and absorption rate of carbon dioxide into 7m monoethanolamine (MEA)/ 2m piperazine (PZ) were measured in a wetted wall column at 40 and 60 °C. The addition of 2m PZ to the 7m MEA increased the absorption rate by a factor of 3 to 5 at 40 °C and 3 to 6 at 60 °C. Absorption rate comparisons in other solvents including 14m diglycolamine®/3.5m morpholine, 5.6m MEA/1.8m PZ, and 5m K⁺/2.5m PZ show rates in 7m MEA/2m PZ that are two to eight orders of magnitude faster depending on the solvent and carbon dioxide partial pressures considered. The equilibrium partial pressure of carbon dioxide over 7m MEA/2m PZ increases with its carbon dioxide loading within the 0.1-0.6 mol CO₂/mol equivalent amine range, as with 7m MEA. Finally, solvent capacity for 7m MEA/2m PZ is greater than 7m MEA by a factor of three.

Contents

FIGURES	V
TABLES	VI
CHAPTER 1 : INTRODUCTION	1
1.1. OVERVIEW	1
1.2. SOLVENTS FOR CO ₂ CAPTURE	2
1.3. MASS TRANSFER WITH FAST CHEMICAL REACTION	3
1.4. PROJECT SCOPE	4
CHAPTER 2 : EXPERIMENTAL METHODS	6
2.1. WETTED-WALL COLUMN.....	6
2.1.1. <i>Equipment Description</i>	6
2.1.2. <i>Gas Analysis</i>	10
2.1.3. <i>Liquid Analysis</i>	10
2.1.4. <i>Physical Mass Transfer Coefficients</i>	11
2.1.4. <i>Experimental Data Analysis</i>	13
2.1. NUCLEAR MAGNETIC RESONANCE SPECTROSCOPY	14
2.2.1. <i>Loading determination by NMR arguments</i>	19
2.3. PHYSICAL PROPERTIES.....	20
2.3.1. <i>Density</i>	20
2.3.2. <i>Viscosity</i>	21
2.3.3. <i>Physical Solubility</i>	21
2.3.4. <i>Diffusion Coefficient</i>	22
2.4. CHEMICALS AND MATERIALS	23
CHAPTER 3 : RESULTS	24
3.1. OVERALL RESULT SUMMARY	24
3.2. SOLUBILITY OF CO ₂ IN 7M MEA/2M PZ	26
3.3. ABSORPTION RATE OF CO ₂ IN 7M MEA/2M PZ	29
CHAPTER 4 : CONCLUSIONS AND RECOMMENDATIONS.....	34
4.1. CONCLUSIONS	34
4.2. RECOMMENDATIONS	34
APPENDIX A : ¹H AND ¹³C NMR SPECTRA.....	36
APPENDIX B : DETAILED RESULTS	45
NOMENCLATURE	50
BIBLIOGRAPHY	52
VITA.....	57

Figures

Figure 1.1 Schematic of CO ₂ Absorber/Stripper	2
Figure 2.1 Detailed Diagram of Wetted-Wall Column	7
Figure 2.2 Schematic of the Wetted-Wall Column Experiment.....	8
Figure 3.1 Graphical Representation of Determining P _{CO₂} * and K _G for 7m MEA/2m PZ at 60°C and Loading = 0.28 mol CO ₂ /equivalent amine.....	25
Figure 3.2 Comparison of CO ₂ VLE in 7m MEA and 7m MEA/2m PZ at 40, 60 °C.....	27
Figure 3.3 CO ₂ Absorption in MEA/PZ blends at 40 °C.....	30
Figure 3.4 CO ₂ Absorption in MEA/PZ blends at 60 °C.....	31
Figure A. 1 ¹³ C NMR Spectrum (Low End) of 7m MEA, $\alpha = 0.57$, T = 27 °C.....	37
Figure A. 2 ¹³ C NMR Spectrum (High End) of 7m MEA, $\alpha = 0.57$, T = 27 °C.....	38
Figure A. 3 Combined ¹ H and ¹³ C NMR Spectrum of 7m MEA, $\alpha = 0.57$, T = 27 °C.....	39
Figure A. 4 ¹³ C NMR Spectrum (Low End) of 7m MEA/2m PZ, $\alpha = 0.30$, T = 27 °C.....	40
Figure A. 5 ¹³ C NMR Spectrum (Intermediate) of 7m MEA/2m PZ, $\alpha = 0.30$, T = 27 °C.....	41
Figure A. 6 ¹³ C NMR Spectrum (High End) of 7m MEA/2m PZ, $\alpha = 0.30$, T = 27 °C.....	42
Figure A. 7 ¹ H and ¹³ C NMR Spectrum of 7m MEA/2m PZ, $\alpha = 0.30$, T = 27 °C.....	43
Figure A. 8 ¹ H NMR Spectrum of 7m MEA/2m PZ, $\alpha = 0.30$, T = 27 °C.....	44

Tables

Table 1.1 Common Amines in Gas Treating.....	3
Table 2.1 Proton and ^{13}C chemical shift summary for 7 m MEA, $\alpha = 0.57$, $T = 25^\circ\text{C}$	15
Table 2.2 Proton and ^{13}C chemical shift summary for 0.6 m PZ, $\alpha = 0.56$, $T = 25^\circ\text{C}$	17
Table 2.3 Proton and ^{13}C chemical shift summary for 7.0m MEA/3.5m PZ, $\alpha = 0.30$, $T = 25^\circ\text{C}$	18
Table 2.4 Density of Partially Loaded 40 wt% MEA at 25°C	20
Table 3.1 Solubility and Rate Summary for CO_2 Absorption in MEA/PZ/ H_2O	26
Table 3.2 Overall Rate Constants for 1.0 M Amines at 25°C (Cullinane, 2005)	33
Table B. 1 7m MEA/2m PZ, $\alpha = 0.28$, $T = 40^\circ\text{C}$, $P_{\text{CO}_2}^* = 51 \text{ Pa}$	46
Table B. 2 7m MEA/2m PZ, $\alpha = 0.37$, $T = 40^\circ\text{C}$, $P_{\text{CO}_2}^* = 207 \text{ Pa}$	46
Table B. 3 7m MEA/2m PZ, $\alpha = 0.57$, $T = 40^\circ\text{C}$, $P_{\text{CO}_2}^* = 11224 \text{ Pa}$	47
Table B. 4 7m MEA/2m PZ, $\alpha = 0.29$, $T = 60^\circ\text{C}$, $P_{\text{CO}_2}^* = 421 \text{ Pa}$	47
Table B. 5 7m MEA/2m PZ, $\alpha = 0.40$, $T = 60^\circ\text{C}$, $P_{\text{CO}_2}^* = 1162 \text{ Pa}$	48
Table B. 6 7m MEA/2m PZ, $\alpha = 0.57$, $T = 60^\circ\text{C}$, $P_{\text{CO}_2}^* = 35725 \text{ Pa}$	48
Table B. 7 7m MEA, $\alpha = 0.35$, $T = 60^\circ\text{C}$, $P_{\text{CO}_2}^* = 212 \text{ Pa}$	49
Table B. 8 7m MEA, $\alpha = 0.43$, $T = 60^\circ\text{C}$, $P_{\text{CO}_2}^* = 8178 \text{ Pa}$	49

Chapter 1 : Introduction

1.1. Overview

Greenhouse gas emissions and their increasing role in global warming has become an issue of much concern in recent times. Amongst the known greenhouse gases, carbon dioxide from combustion of fossil fuels accounts for 96% of the total emissions in the U.S., with approximately 36% of total CO₂ emissions originating from electricity generation in coal-fired power plants (EPA, 2002). Consequently, modern research geared towards developing new CO₂ capture technologies is ongoing worldwide.

Traditionally, absorption/stripping via circulated aqueous alkanolamines has been the most favored technology for removing CO₂ from process and waste gas streams. It has applications in ammonia manufacturing, synthesis gas production, natural gas treating, and ethylene manufacturing, among others.

Figure 1.1 shows a typical process schematic for CO₂ capture using an aqueous amine such as monoethanolamine (MEA). In this set-up, the CO₂-containing waste gas stream enters the bottom of the packed or tray absorber where it counter-currently contacts and reacts with the amine solvent. The treated gas stream exits the top of the absorber whereas the rich amine solvent exits the bottom and then continues to the cross-exchanger for pre-heating, and finally onto the stripper. Heat supplied by steam from a reboiler is applied to the loaded solvent in the stripper for regeneration. The hot lean solvent is recycled to absorber via the cross-exchanger, and a cooler. The lean solvent

serves as a heating medium for the rich solvent in the cross-exchanger. Finally, the captured gases are removed from the top of the stripper for disposal or storage.

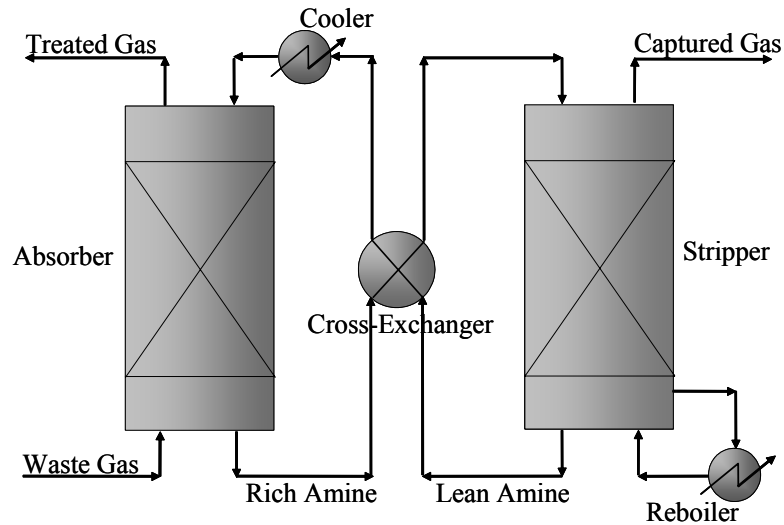



Figure 1.1 Schematic of CO₂ Absorber/Stripper

Flue gas from coal-fired power plants has an inlet CO₂ concentration of 10-15 vol% with total pressure of that hovers around one atmosphere. The captured gas concentration should be 1-1.5 vol% range, depending on the downstream process requirements. The absorber and stripper are typically operated at 40-60 °C and 100-120 °C, respectively.

1.2. Solvents for CO₂ Capture

Many solvents have been researched for potential commercial use to remove CO₂ from flue gas streams. However, aqueous amines are considered to be the most effective because of their relatively high absorption rates. Currently, 7m MEA is considered the state-of-technology; it has been applied in small plants for CO₂ recovery from flue gas. Table 1.1 displays some of the common amines used in gas treating.

Table 1.1 Common Amines in Gas Treating

Name(Abbr.)	Structure
Monoethanolamine (MEA)	$\text{HO}-\text{CH}_2-\text{CH}_2-\text{N} \begin{matrix} \text{H} \\ \text{H} \end{matrix}$
Diglycolamine® (DGA)	$\text{HO}-\text{CH}_2-\text{CH}_2-\text{O}-\text{CH}_2-\text{CH}_2-\text{N} \begin{matrix} \text{H} \\ \text{H} \end{matrix}$
Diisopropanolamine (DIPA)	$\begin{matrix} \text{CH}_3 & & \text{CH}_2 & & \text{CH}_2 & & \text{CH}_3 \\ & \diagdown & & \diagup & & \diagdown & \\ & \text{CH} & & \text{N} & & \text{CH} & \\ & & & & & & \\ & \text{OH} & & \text{H} & & \text{OH} & \end{matrix}$
Methyldiethanolamine (MDEA)	$\begin{matrix} \text{HO}-\text{CH}_2-\text{CH}_2- \\ \text{HO}-\text{CH}_2-\text{CH}_2- \end{matrix} \text{N}-\text{CH}_3$
Piperazine (PZ)	

1.3. Mass Transfer with Fast Chemical Reaction

Carbon dioxide absorption by alkanolamines is a process that involves complex mass transfer accompanied by fast chemical reaction. The difficulty associated with accurately representing this process analytically has led to the development several approximations including the pseudo-first order model. It assumes the liquid phase CO_2 concentration in the boundary layer is constant and can be represented by bulk liquid CO_2 concentration. Therefore, the need to track speciation in the boundary layer is removed.

For a reversible reaction of involving amine and carbon dioxide, the concentration profile of the reacting CO_2 in the boundary layer can be represented by

$$D_{\text{CO}_2} \frac{\partial^2 [\text{CO}_2]}{\partial x^2} - k_2 [\text{Am}] [\text{CO}_2] = 0 \quad (1.1)$$

Applying the pseudo-first order approximation by assuming that the amine concentration in the boundary layer is constant and equal to the bulk liquid concentration yields

$$D_{CO_2} \frac{\partial^2 [CO_2]}{\partial x^2} - k_l [CO_2] = 0 \quad (1.2)$$

where k_2 and k_l are the second order and pseudo-first order rate constants.

The solution to Equation 1.2 is

$$N_{CO_2} = \frac{\sqrt{D_{CO_2} k_2 [Am]_b}}{H_{CO_2}} (P_{CO_2} - P_{CO_2}^*) = k_g' (P_{CO_2} - P_{CO_2}^*) \quad (1.3)$$

where k_g' is the normalized flux (See Section 2.1.5.).

1.4. Project Scope

Several amine blends have been used industrially to removal of CO₂ from process gases. Most effective blends often include a primary or secondary amine (such as MEA, DGA or DEA, DIPA), which possess a high reaction rate, and a tertiary amine (such as MDEA) which exhibits a low heat of reaction. A high reaction rate is desirable because it increases CO₂ flux into solution thereby decreasing the number of equilibrium stages required achieve a specified separation. Furthermore, a low heat of reaction is critical because it minimizes the energy required to regenerate the solvent in the stripper.

Bishnoi (2000), Dang (2001), Aboudheir (2003), and Al Juaied (2004) measured VLE and absorption rates of CO₂ in MDEA/PZ, MEA/PZ, MEA, and DGA/MOR respectively, at different amine concentrations. MEA/PZ is of particular interest because piperazine has a high apparent second order rate constant and two amine groups per molecule. This feature makes it a good promoter of absorption when added to a primary amine, such as MEA, because it is expected to absorb CO₂ at a faster rate with the same amine concentration as just aqueous MEA.

Dang (2001) measured VLE and absorption rates for PZ promoted MEA 0.4m MEA/0.6m PZ – 5.6m MEA/1.8m PZ range. It was found that absorption rates progressively increased with increased PZ concentration and total amine concentration. This work extends Dang's work by measuring VLE absorption rates at various CO₂ loadings for 7m MEA/2m PZ at absorber conditions. 7m MEA/2m PZ was chosen in this study because 7m MEA represents the state-of-art technology and 2m PZ is soluble in 7m MEA at about 60 °C. In other words, the upper limit on attainable technological improvements over the baseline solvent can be determined. The results were also compared to previous work performed by other researchers for different solvents. In addition, Nuclear Magnetic Resonance (NMR) was used in an attempt to better understand CO₂ speciation in 7m MEA/2m PZ.

Chapter 2 : Experimental Methods

This chapter discusses the experimental methods and equipment used in measuring the behavior of MEA/PZ mixtures, including methods employed in data analysis and physical property estimation. Equilibrium partial pressure of CO₂ and rate of absorption of CO₂ in MEA/PZ were estimated with the aid of a wetted-wall column. Further, an attempt to measure speciation of MEA/PZ in CO₂ with Nuclear Magnetic Resonance (NMR) spectroscopy is presented.

2.1. Wetted-Wall Column

The wetted-wall column (Figure 2.1) used in this work for determining vapor-liquid equilibrium and CO₂ absorption rates was also used by Mshewa (1995), Bishnoi (2000), Dang (2001), and Cullinane (2005).

2.1.1. Equipment Description

The wetted-wall column is a stainless steel tube 9.1 cm long with outer and hydraulic diameters of 1.26 cm and 0.44 cm, respectively. The total gas-liquid contact area is 38.52 cm², consisting of a longitudinal area of 36.03 cm² and another 2.49 cm² representing the area for the top hemispherical portion of the tube. The tube is encapsulated by a thick-walled glass cylinder with an outside diameter of 2.54 cm, giving a gas flow cross-sectional area of 3.82 cm². The inner encapsulation is embedded in yet

another thick-walled glass cylinder with an outer diameter of 10.16 cm. Heated silicone oil is circulated in the space between the two chambers to fix temperatures during experimentation.

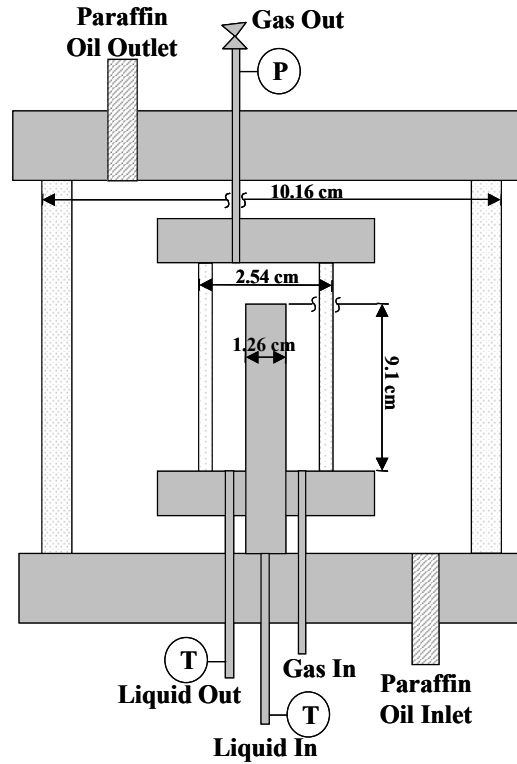


Figure 1.1 Detailed Diagram of Wetted-Wall Column

Figure 2.2 shows the entire experimental schematic. The liquid solution was stored in a reservoir with a total volume of 1.4 liters. The reservoir was constructed as modified calorimetric bombs which were connected in series. The liquid was continuously pumped in a closed loop through the reservoir, heated coil bath, and the wetted-wall column. The liquid flowed up through the middle of stainless steel tube contactor where it then overflowed at the top and then formed a thin, consistent liquid film on the surface of the gas-liquid contactor.

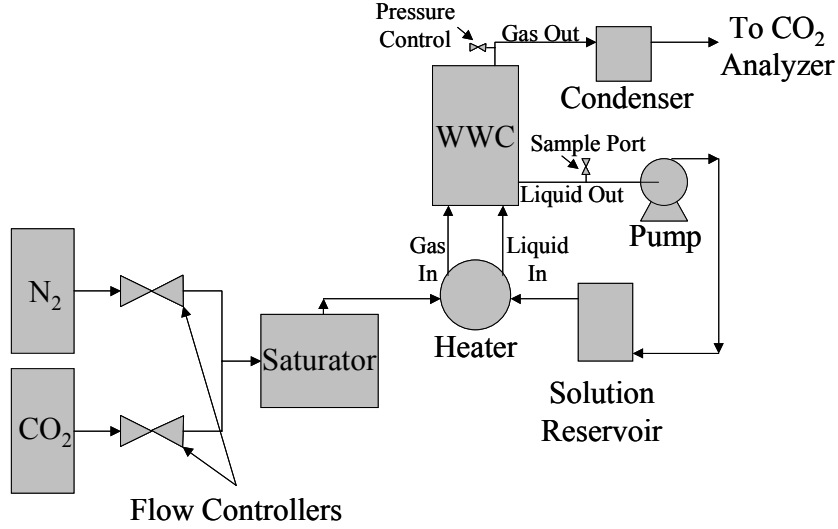


Figure 2.2 Schematic of the Wetted-Wall Column Experiment

The liquid flowrate was regulated with a rotameter. Cullinane (2005) calibrated the liquid rotameter with water, yielding the following equations:

$$Q_{w,T_{ref}} (cm^3/s) = 0.4512x - 0.2901, \quad (2.1)$$

$$Q_{sol,T_{ref}} (cm^3/s) = Q_{w,T_{ref}} \sqrt{\frac{(7.83 - \rho_{T_{ref}})}{(7.83 - 0.997)\rho_{T_{ref}}}}, \quad (2.2)$$

$$Q_{sol} (cm^3/s) = Q_{sol,T_{ref}} \sqrt{\frac{7.83 - \rho^2}{7.83 - \rho_{T_{ref}}^2}}, \quad (2.3)$$

where Q_w represents the volumetric flowrate of water, Q_{sol} is the volumetric flowrate of the solution, ρ is the density of the solution in g/cm^3 , and x is the rotameter reading. The value of 7.83 represents the density of the rotameter float. The subscript T_{ref} refers to the value at a standard temperature of 25°C. The liquid temperature was measured at the inlet and outlet of the contactor by Type-J thermocouples within $T \pm 1.0$ °C.

Nitrogen and carbon dioxide gases (> 99% pure) were metered from storage cylinders to apparatus by Brooks mass flow controllers. A 20 SLPM controller (S/N

8708HCO99980) was used for N₂ gas whereas two other controllers, a 2 SLPM controller (S/N 9310HCO38406102) and the other, a 100 SCCM controller (S/N 9103HCO370444) were available for CO₂ supply. Two Omega FL-100 high accuracy shielded rotameters were used for gas metering, specifically for the 7m MEA/2m PZ data points for 40 and 60 °C at 0.57 CO₂ loading. Calibration curves for N₂ and CO₂ flow were provided by Omega Instruments at specified experimental conditions.

The gases were mixed and pre-saturated with water at the column operating temperature in a sealed vessel immersed in a heat bath. The sealed vessel contained approximately 500 cm³ of water with a height of about 5 inches. The resulting gas stream was then introduced into the bottom end of the contacting chamber via a 1/8 inch tube. The gas stream counter-currently contacts overflowing liquid film on the contactor's surface, after which, the final gas mixture exits through another 1/8 inch tube at the top of the contacting chamber. Subsequently, the exited gas mixture is routed to a condenser (1L Erlenmeyer flask submerged in an ice bath), where its water vapor condenses and is allowed to settle in the bottom of the flask. The partially dry gas mixture then exits through the top of the condenser. The emergent gas stream at a volumetric flow rate of 5-6 SLPM is vented in the lab hood, leaving 300-500 cm³/min of gas flow. This remnant gas flow is then channeled to a drying column containing magnesium perchlorate to remove excess moisture. Finally, the dry gas stream was sent to Horiba gas analyzers to determine the CO₂ concentration of the dry gas stream.

Column pressure was regulated by means of a needle valve on the gas outlet line from the wetted-wall column and monitored by an analog pressure gauge (Omega, P/N

PGM-100L-60) to an accuracy of ± 0.5 psig. System pressure for this work ranged from 30-50 psig.

2.1.2. Gas Analysis

The method for gas analysis used in this work is identical to Cullinane (2005). The concentration of CO₂ in the outlet gas was measured by Horiba PIR-2000 gas analyzers. The available range of the analyzers was adjustable, varying from 0.05 to 25 vol%, with an expected accuracy of 1% of full scale. The equipment uses IR spectroscopy to measure the amount of CO₂ in the gas phase. The analyzers were calibrated prior to each experiment by bypassing the wetted-wall column and adjusting the CO₂ flow rate in the feed gas to give known concentrations. A chart recorder was used during the calibrations and experiments to record the response of the analyzers. Readings from the recorder are expected to be accurate to 0.2% of full scale.

2.1.3. Liquid Analysis

In order to determine the CO₂ composition in the liquid phase, samples were withdrawn from a septum on the liquid outlet tubing by a 150 μ L syringe. First, the samples were diluted by placing 50 μ L of sample in 10 mL DI H₂O. For analysis, the diluted samples were injected into 30 wt% H₃PO₄ sparged with nitrogen. The acid liberated all inorganic carbon from the solution and the nitrogen sweep gas (~ 0.5 L/min) carried the gas phase to the Horiba PIR-2000 gas analyzer (range 0.05 vol%). The gas stream was passed through a drying column of magnesium perchlorate prior to entering the analyzers.

Prior to each use, the liquid analysis method was calibrated by injecting several known volumes of freshly-prepared 7 mM Na₂CO₃. In general, 50, 100, 150, and 200 µL volumes were used to obtain a calibration curve for the analyzer response. During the calibration and the experiments, the response was recorded on a chart recorder. The sharp peaks obtained were proportional to the liquid phase CO₂ concentration. In this way, the corresponding liquid phase concentrations were determined.

2.1.4. Physical Mass Transfer Coefficients

2.1.4.1. Gas Film Mass Transfer Coefficient

Bishnoi (2000) provided a correlation for deriving the gas film mass transfer coefficient, k_g , for the wetted-wall column based on SO₂ absorption experiments into 0.1 M NaOH.

$$Sh = 1.075 \left(Re Sc \frac{d}{h} \right)^{0.85} \quad (2.4)$$

Reynolds and Schmidt numbers are defined as follows:

$$Re = \frac{u \rho d}{\mu} \quad (2.5)$$

$$Sc = \frac{\mu}{\rho D_{CO_2}} \quad (2.6)$$

where u is the linear velocity of the gas, ρ is the density, and μ is the viscosity. The other parameters d , h , and D_{CO_2} represent the hydraulic diameter of the annulus (0.44 cm), height of stainless steel contactor (9.1 cm), and diffusivity of CO₂ in nitrogen, respectively. Hence, the gas film mass transfer coefficient can be calculated from the Sherwood number given as:

$$Sh = \frac{RTk_g d}{D_{CO_2}} \quad (2.7)$$

where T is the temperature and R is the gas constant. The data points presented in this work had resistances that were mostly between 20 to 70% gas film controlled.

2.1.4.2. Liquid Film Mass Transfer Coefficient

The liquid film mass transfer coefficient was derived from a correlation based on falling-film theory as developed by Pigford (1941). Pigford's model utilized a momentum balance as presented by Bird *et al.* (1960) to determine film thickness, δ , and surface velocity, u_s . The liquid mass transfer coefficient, k_l^o is given as follows:

$$k_l^o = \frac{Q_{sol}}{A} (1 - \Theta), \quad (2.8)$$

where A is the contact area of mass transfer and Θ represents a dimensionless driving force of the diffusing gas in the liquid film, calculated as follows:

$$\Theta = \frac{[CO_2]_i - [CO_2]_o^{out}}{[CO_2]_i - [CO_2]_o^{in}} = 0.7857 \exp(-5.121\eta) + 0.1001 \exp(-39.21\eta) + 0.036 \exp(-105.6\eta) + 0.0181 \exp(-204.7\eta), \text{ for } \eta > 0.01 \quad (2.9)$$

$$\Theta = 1 - 3\sqrt{\frac{\eta}{\pi}}, \text{ for } \eta < 0.01, \quad (2.10)$$

where $[CO_2]_o^{in}$ and $[CO_2]_o^{out}$ represent the concentration of CO_2 in the bulk liquid at the inlet and outlet of the wetted-wall column, respectively, and $[CO_2]_i$ is the concentration of CO_2 at the gas-liquid interface. η is a dimensionless penetration distance defined as

$$\eta = \frac{D_{CO_2} \tau}{\delta^2}, \quad (2.11)$$

and τ is the surface contact time, defined as

$$\tau = \frac{h}{u_s}. \quad (2.12)$$

The surface velocity, u_s , and film thickness, δ , are given by

$$u_s = \frac{\rho g \delta^2}{2\mu}. \quad (2.13)$$

$$\delta = \sqrt[3]{\frac{3\mu Q_{sol}}{\rho g W}}, \quad (2.14)$$

where μ is the liquid viscosity, Q_{sol} is the volumetric flowrate of the liquid, ρ is the liquid density, D_{CO_2} is the CO_2 diffusivity in the liquid, g is the gravity constant and W is the circumference of the column.

2.1.4. Experimental Data Analysis

Five to seven data points were taken during each experiment. Each data point was obtained by varying the bulk gas partial pressure of CO_2 . The flux of CO_2 into or out of the liquid phase can be derived from the following expressions:

$$N_{CO_2} = K_G (P_{CO_2,b} - P_{CO_2}^*) \quad (2.15)$$

$$P_{lm} = \frac{P_{CO_2,in} - P_{CO_2,out}}{\ln(P_{CO_2,in}/P_{CO_2,out})} \quad (2.16)$$

The log mean average bulk CO_2 partial pressure, P_{lm} , was used to approximate the bulk CO_2 partial pressure. Further, the overall mass transfer coefficient, K_G can be obtained graphically from the slope of CO_2 flux and the P_{lm} . The equilibrium partial pressure, $P_{CO_2}^*$, is calculated by interpolation. Typically, the three points that bracket equilibrium are used. The partial pressure that corresponds to zero flux represents $P_{CO_2}^*$.

The normalized flux or modified liquid phase mass transfer coefficient, k_g' , was calculated as:

$$k_g' = \left(\frac{1}{K_G} - \frac{1}{k_g} \right)^{-1} \quad (2.17)$$

The normalized flux accounts for both physical mass transfer and chemical kinetics of absorption. This feature is particularly important because it allows an effective way for quantifying the effect of chemical reactions in amine absorption processes.

2.1. Nuclear Magnetic Resonance Spectroscopy

NMR experiments can provide detailed information about the liquid phase composition of various amine systems. Carbon-13 and proton NMR were employed in this work in an attempt to understand speciation and quantify the various ionic species that are present in a monoethanolamine-piperazine-carbon dioxide solvent system.

A Varion INOVA 500 NMR was used for the analysis. The samples were prepared by mixing required quantities of MEA, PZ, and DI H₂O (about 25% of the water required was substituted with D₂O). After complete dissolution of solid components upon gentle heating, the sample was then introduced into an NMR tube, and subsequently saturated with 99% ¹³CO₂ from Cambridge Isotope Laboratories by sparging a steady very low-pressure stream of the gas into the NMR tube. The resulting samples were sealed off in the NMR tubes by a simple glass blowing technique prior to ambient temperature analysis at the University of Texas NMR Lab in the Department of Chemistry.

Tables 2.1 and 2.2 summarize the ^{13}C and ^1H NMR shifts for 7m MEA at 0.57 loading and 0.6m PZ at 0.56 loading, both at 25°C. Table 2.2 is adapted from Bishnoi (2000).

Table 2.1 Proton and ^{13}C chemical shift summary for 7 m MEA, $\alpha = 0.57$, $T = 25^\circ\text{C}$

^1H Peaks			^{13}C Peaks		
Shift (ppm)	Area	Species	Shift (ppm)	Area	Species
2.61	1.88	Protons on C next to nitrogen (MEA/MEA H^+)	41.39	34.72	C next to nitrogen (MEA/MEA H^+)
2.64	1.05	Protons on C next to nitrogen (MEACOO $^-$)	43.28	18.29	C next to nitrogen (MEACOO $^-$)
3.08	1.00	Protons on C next to OH group (MEACOO $^-$)	57.82	36.71	C next to OH group (MEA/MEA H^+)
3.29	1.88	Protons on C next to OH group (MEA/MEA H^+)	61.31	19.78	C next to OH group (MEACOO $^-$)
-	-	-	158.37	27.94	Possibly CO $_2$ (g)
-	-	-	159.28	22.54	Possibly CO $_2$ (aq)
-	-	-	160.66	644.26	HCO $_3^-$ /CO $_3^{2-}$
-	-	-	164.45	1000.00	Carbamate C

Ideally, it is expected that NMR spectrum for the amine blend should cleanly mirror the combination of the individual spectrum for single solvent systems. However, it is found that there is a considerable amount of overlap in spectrum for MEA/PZ systems. Table 2.3 displays ^{13}C and ^1H NMR shifts for 7m MEA/3.5m PZ at a loading of 0.30 and 25°C and clearly depicts this overlap phenomenon. Although the protons on the carbons

next to the NH/H^+ group and the protons on the carbons next to the carbamate for the PZ/PZH^+ carbamate species were identified via proton NMR, it was not possible to conclusively identify the corresponding carbons using ^{13}C NMR. However, it is believed that piperazine carbamate ring carbons (Cs closer to the carbamate and to amine group) show up at about 42.22 ppm on the ^{13}C spectrum as a combined peak. All relevant NMR spectra are included in Appendix A.

Table 2.2 Proton and ^{13}C chemical shift summary for 0.6 m PZ, $\alpha = 0.56$, $T = 25^\circ\text{C}$ (Bishnoi, 2000)

^1H Peaks			^{13}C Peaks		
Shift (ppm)	Area	Species	Shift (ppm)	Area	Species
2.83	1.02	Protons on ring C next to amine/amineH ⁺ in PZ/PZH ⁺ Carbamate	42.12	4.08	ring C next to N in PZ/PZH ⁺ Carbamate (closer to COO ⁻)
2.84	1.30				
2.85	1.14				
2.90	12.84	PZ/PZH ⁺ ring Cs protons	42.63	14.90	PZ/PZH ⁺ ring Cs
3.15	0.74	PZ Dicarb. ring protons	43.59	4.41	ring C next to amine/amineH ⁺ in PZ/PZH ⁺ Carbamate
3.34	1.08	H on ring C next to N in PZ/PZH ⁺ Carbamate (closer to COO ⁻)			
3.36	1.31				
3.37	1.02		44.10	0.92	PZ Dicarb. ring Cs
	-				C next to OH group (MEACOO ⁻)
	-	-	161.63	0.15	HCO ₃ ⁻ /CO ₃ ²⁻
-	-	-	162.37	0.84	Carbamate C
-	-	-	163.01	0.16	Dicarbamate Cs
-	-	-	164.45	1000.00	
-	-	-			

**Table 2.3 Proton and ^{13}C chemical shift summary for 7.0m MEA/3.5m PZ, $\alpha = 0.30$,
T = 25°C**

¹ H Peaks			¹³ C Peaks					
Shift (ppm)	Area	Species	Shift (ppm)	Area	Species			
2.49	66.64	PZ Dicarb. ring protons	40.88	37.74	PZ/PZH ⁺ ring Cs			
2.54		Protons on C next to nitrogen (MEA/MEAH ⁺)	43.12	43.05	PZ Dicarb. ring Cs			
2.55			55.23	61.95	C next to nitrogen (MEACOO ⁻)			
2.56								
2.63	79.05	Protons on C next to nitrogen (MEACOO ⁻)	55.43	4.42	C next to nitrogen (MEA/MEAH ⁺)			
2.64			55.75	67.36	C next to OH group (MEA/MEAH ⁺)			
2.65								
2.78	45.01	Protons on ring C next to amine/amineH ⁺ in PZ/PZH ⁺ Carbamate	56.28	3.01	C next to OH group (MEACOO ⁻)			
2.96			158.13	80.54	HCO ₃ ⁻ /CO ₃ ²⁻			
3.18			160.26	1000.00	PZ Dicarbamate Cs			
3.19			161.77 (~162)	1571.96	MEA Carbamate C PZ/PZH ⁺ Carbamate			
3.21	73.86	Protons on C next to OH group(MEA/MEAH ⁺)						
3.22								
3.23								
3.51	1.02					H on ring C next to N in PZ/PZH ⁺ Carbamate (closer to COO-)		
3.32								

2.2.1. Loading determination by NMR arguments

A simple method of determining loading from ^{13}C NMR peak areas was developed. The concept stems from a mass balance on the carbon dioxide introduced into sample solution. Loading is defined below as:

$$\alpha = \frac{M_{\text{CO}_2}}{M_{\text{amine}}} \quad (2.18)$$

M_{CO_2} refers to moles of carbon dioxide and M_{amine} , moles of amine equivalent in solution. M_{CO_2} is calculated by summing the peak areas for all resulting species from reactions with $^{13}\text{CO}_2$. For example, for the 7.0m MEA/3.5m MEA case, the species include MEACOO^- , $\text{HCO}_3^-/\text{CO}_3^{2-}$, PZCOO^- , and $\text{PZ}(\text{COO}^-)_2$. The sum is then scaled down to a $^{12}\text{CO}_2$ basis using a $^{12}\text{C}:^{13}\text{C}$ ratio of 1.8:100 (deemed appropriate for samples in this work). Similarly, M_{amine} is calculated by adding all the peak areas for the native carbon species i.e. peaks in the low chemical shift range in the ^{13}C NMR spectrum (< 150 ppm). To obtain the amine equivalent, the resulting sum is further divided by two since there are two C atoms for each N atom in both MEA and PZ molecules. With both M_{CO_2} and M_{amine} determined, loading can hence be calculated. With this algorithm the loading for 7.0 m MEA/3.5m PZ sample was determined as approximately 0.3.

2.3. Physical Properties

2.3.1. Density

Dang (2001) approximated the density of loaded MEA/PZ blends with the same total amine concentrations as MEA by using Weiland (1996) experimental density data for various partially loaded MEA solutions at ambient conditions. It was determined from rudimentary calculations, in this work, that 40 wt% MEA contains approximately the same total amine concentration as 7m MEA/2m PZ. Hence, Weiland's density data for partially loaded 40 wt% MEA was used herein to approximate the density of the blend.

Table 2.4 Density of Partially Loaded 40 wt% MEA at 25°C

Loading (mol CO₂/mol equivalent amine)	Density (g/mL)
0.00	1.017
0.05	1.032
0.10	1.043
0.15	1.056
0.20	1.070
0.25	1.082
0.30	1.096
0.35	1.114
0.40	1.126
0.45	1.139
0.50	1.147

2.3.2. Viscosity

Viscosity was determined by a correlation developed by Weiland (1996) for MEA as a function of loading, amine fraction, and temperature. Similarly, this correlation was subsequently used to approximate the viscosity of partially loaded 7m MEA/2m PZ with the same total amine concentration as MEA.

$$\frac{\mu}{\mu_w} = \exp \frac{[(aw + b)T + (cw + d)][\alpha(ew + fT + g) + 1]w}{T^2} \quad (2.19)$$

$$\ln \mu_w = -46.288 + \frac{3703.7}{T} + 5.924 \ln T \quad (2.20)$$

where μ and μ_w are the viscosities of the amine solution and water, respectively (mPa.s), w is the weight percent amine, T (K) is temperature, and α is the loading. The empirical coefficients are as follows $a = 0$, $b = 0$, $c = 21.186$, $d = 2373$, $e = 0.01015$, $f = 0.0093$, and $g = -2.2589$.

2.3.3. Physical Solubility

Due to high reactivity of CO_2 with amines, it is impossible to determine a true physical solubility. It is known that N_2O , a molecule with an identical molecular weight and a similar Lennard Jones potential, can be used to predict the behavior of CO_2 in the liquid phase (Clarke, 1964). Clarke concluded that the ratio of CO_2 to N_2O solubility is constant for systems. Hence, for all practical purposes, the ratio of the solubility of CO_2 in any amine to the solubility of N_2O in the same amine is equal to the same ratio in water. Therefore,

$$H_{\text{CO}_2, \text{Am}} = H_{\text{N}_2\text{O}, \text{Am}} \left(\frac{H_{\text{CO}_2, w}}{H_{\text{N}_2\text{O}, w}} \right) \quad (2.21)$$

The Henry's constants for CO₂ and N₂O in water as correlated by Versteeg and van Swaaij (1988b) are:

$$H_{CO_2,w} \left(\frac{mol}{L \cdot Pa} \right) = 3.54 \times 10^{-4} \exp \left(\frac{2044}{T(K)} \right) \quad (2.22)$$

$$H_{N_2O,w} \left(\frac{mol}{L \cdot Pa} \right) = 1.17 \times 10^{-4} \exp \left(\frac{2284}{T(K)} \right) \quad (2.23)$$

Weiland (1996) confirmed that the Henry's constant of N₂O in MEA was a linear function of loading. Further, the slopes for H vs. loading for 10, 20, 30, and 40 wt% MEA were approximately equal, with their intercepts increasing with aqueous MEA concentration. Goel (2005) measured the Henry's constant of N₂O in 7m MEA/2m PZ at a CO₂ loading of 0.2. This value (H = 5333 kPa.m³/kmol) agreed with Weiland's value at $\alpha = 0.2$ for 20 wt% MEA to within 5%. As a result, Weiland data for partially loaded 20 wt% MEA was interpolated to yield the Henry's constants used in this work for 7m MEA/2m PZ. In so doing, a linear dependence of Henry's law constants for 7m MEA/2m PZ on loading was similarly assumed.

2.3.4. Diffusion Coefficient

Pacheco (1998) correlated experimental data obtained by Versteeg and van Swaaij (1988b) and Tamimi et al. (1994a, 1994b) to derive CO₂ diffusivities in water and N₂O diffusivities both water and amines. The correlations, which are also based on N₂O analogy, are as follows:

$$D_{CO_2,w} (cm^2/s) = 0.02397 \exp \left(\frac{-2122.2}{T(K)} \right) \quad (2.24)$$

$$D_{N_2O,w} (cm^2/s) = 0.04041 \exp\left(\frac{-2288.4}{T(K)}\right) \quad (2.25)$$

$$D_{N_2O,Am} (cm^2/s) = 5.533 \times 10^{-8} \frac{T(K)}{\mu(cP)^{0.545}} \quad (2.26)$$

Therefore, the diffusivity of CO₂ in amine can be estimated by:

$$D_{CO_2,Am} = D_{N_2O,Am} \frac{D_{CO_2,w}}{D_{N_2O,w}}. \quad (2.27)$$

2.4. Chemicals and Materials

Monoethanolamine [141-43-5] (>99%) was purchased from Huntsman Chemicals and Anhydrous piperazine [110-85-0] (>99%) was purchased from Sigma-Aldrich. Deuterium oxide (D₂O) [7789-20-0], 99.9%, and carbon-13 gas [1111-72-4], (99% purity) used in the NMR experiments was obtained from Cambridge Isotope Laboratories, Inc.

Nitrogen [7727-37-9] used in all experiments was >99% pure and was supplied by the Department of Physics at The University of Texas at Austin. Carbon dioxide (>99% pure) [124-38-9] was purchased from Matheson Tri-gas.

Chapter 3 : Results

Solubility and absorption rate results for 7m monoethanolamine/2m piperazine and for 7m monoethanolamine are discussed. The experiments were performed with a wetted-wall column at 40 and 60 °C with solvent concentration ranging from 0.2 to 0.6 moles CO₂/equivalent amine.

3.1. Overall Result Summary

Equilibrium partial pressure, $P_{CO_2}^*$ was derived at the point of zero flux on a plot of CO₂ flux versus log mean partial pressure as exemplified in Figure 3.1. The three points that bracket equilibrium were used in the calculation of $P_{CO_2}^*$, in this case, equals 420 Pa.

The slope of the line which represents the overall mass transfer coefficient, K_G was used in the calculation of normalized flux, k_g' according to Equation 3.1

$$\frac{1}{k_g'} = \frac{1}{K_G} - \frac{1}{k_g} \quad (3.1)$$

The gas film mass transfer coefficient, k_g was determined from a Sherwood number correlation for the wetted-wall column (Equation 2.7). The percent gas phase transfer resistance, K_G/k_g , represents the amount of mass transfer resistance attributable to the gas phase. A value greater than 50% indicates that much of the resistance lies in the gas phase diffusion of CO₂ to the interface. Therefore, low K_G/k_g values (< 50%) are

desirable because they insure that k_g' is a more accurate representation of the effect of chemical reaction in the mass transfer process.

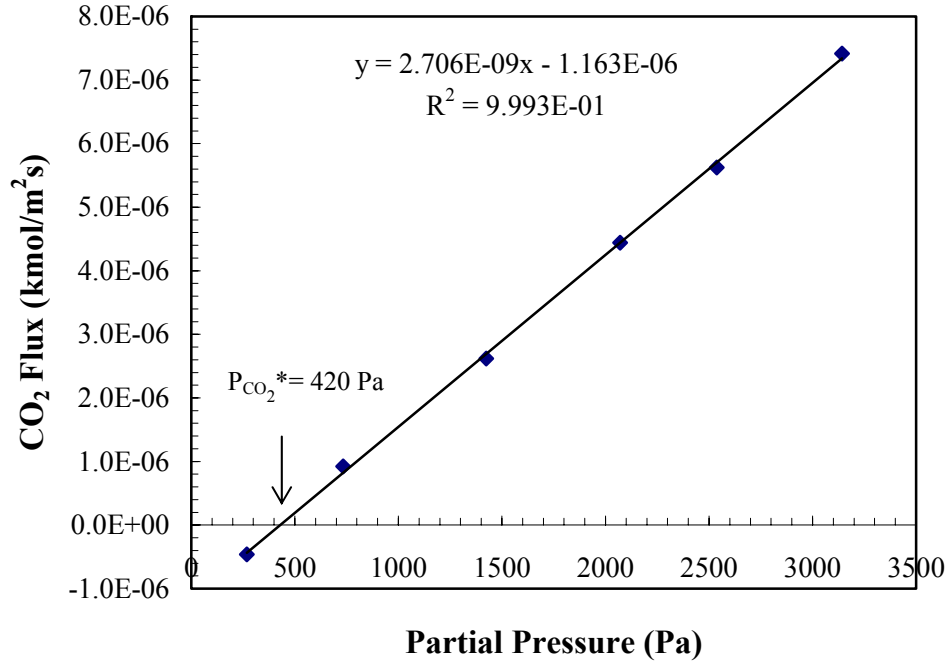


Figure 3.1 Graphical Representation of Determining $P_{CO_2}^*$ and K_G for 7m MEA/2m PZ at 60°C and Loading = 0.28 mol CO₂/equivalent amine

Table 3.1 summarizes the experimental conditions and key results. Since experimental data is sufficiently available at 60°C in the literature for 7m MEA, experiments were performed for 7m MEA as a way to validate the wetted-wall column experimental methods. Overall experimental results are summarized in Table 3.1. Detailed results are included in Appendix B.

Data points with percent gas phase transfer resistance of 40 to 75% show k_g' errors of up to 20% whereas the data point with K_G/k_g of 93% contains an error in k_g' that

could be significantly greater than 50%. The errors in the equilibrium partial pressures calculated in this work are to the order of 10 to 15%.

Table 3.1 Solubility and Rate Summary for CO₂ Absorption in MEA/PZ/H₂O

T(°C)	Amine (m)		Loading (mol CO ₂ /equivamine)	P _{CO₂} * (Pa)	10 ⁹ .k _g ' (kmol/m ² .s.Pa)	k _l ^o (cm/s)	K _G /k _g
	MEA	PZ					
40	7	2	0.28	51	7.4	0.00521	0.69
40	7	2	0.37	207	13	0.00523	0.75
40	7	2	0.57	11200	1.3	0.00534	0.47
60	7	2	0.29	420	11	0.00602	0.76
60	7	2	0.40	1160	9.9	0.00595	0.68
60	7	2	0.57	35700	1.4	0.00618	0.41
60	7	0	0.36	212	46*	0.00806	0.93*
60	7	0	0.43	8180	1.7	0.00747	0.41

* indicates potentially greater error in k_g'

3.2. Solubility of CO₂ in 7m MEA/2m PZ

Dang (2001) fitted the data of Jou *et al.* (1995) for CO₂ solubility in 7m MEA to a simple vapor liquid equilibrium model which accounts for speciation in the MEA/H₂O system. The P_{CO₂}* predicted by Dang for 7m MEA is compared to experimental VLE data obtained in this work for 7m MEA/2m PZ in Figure 3.2.

The equilibrium partial pressure of CO₂ in 7m MEA/2m PZ increases like that in 7m MEA with increasing CO₂ loading at both temperatures although the experimental data series show different slopes. The general trend is that at low loading ($\alpha < 0.5$), P_{CO₂}* for the blend is elevated when compared to 7m MEA at both 40 and 60 °C. On the other hand, at higher loading ($\alpha > 0.5$), there appears to be a slight depression in P_{CO₂}* for 7m MEA/2m PZ when compared to 7m MEA.

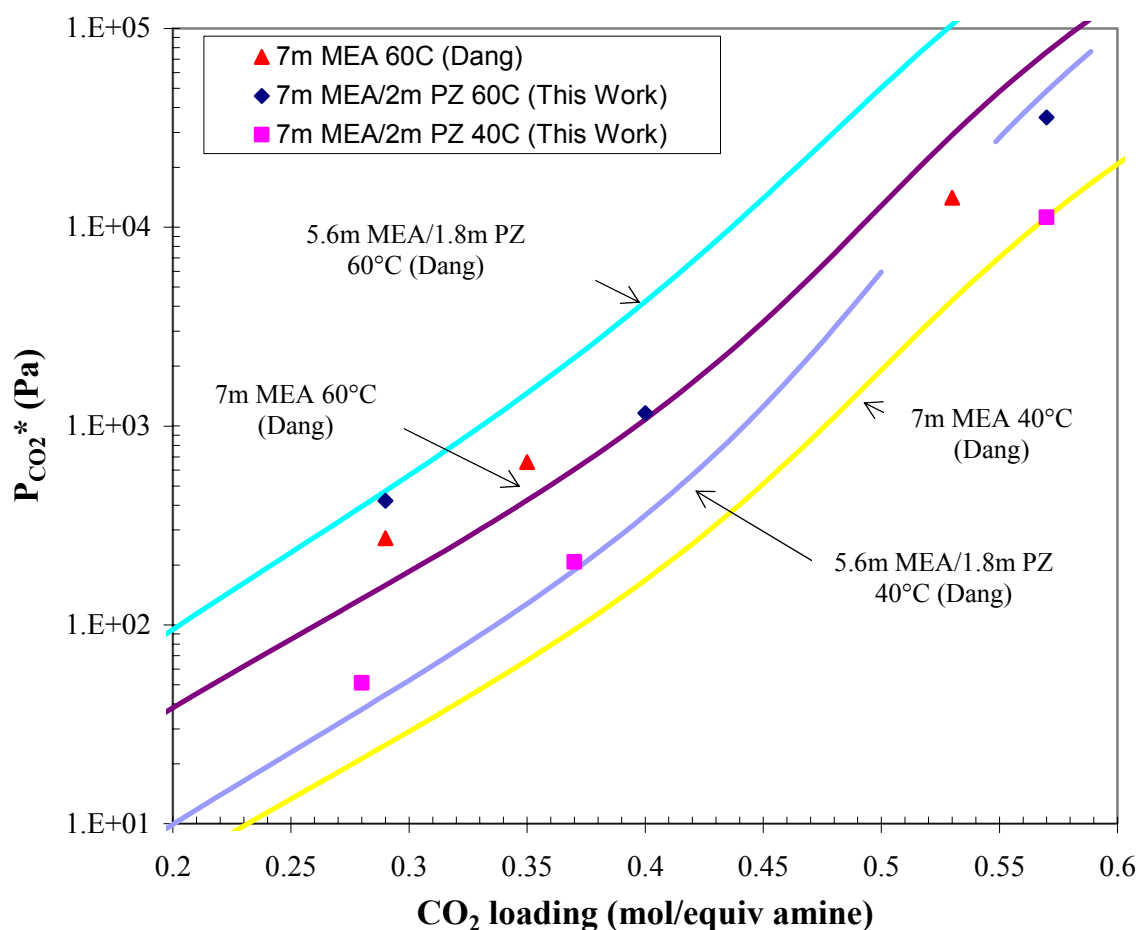
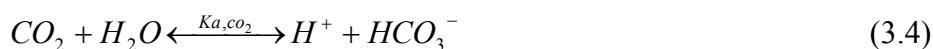


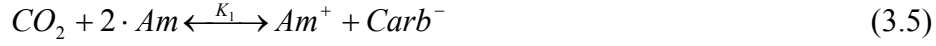
Figure 3.2 Comparison of CO₂ VLE in 7m MEA and 7m MEA/2m PZ at 40, 60 °C

Points: Experimental Data; Lines: Model Prediction by Dang (2001)

A plausible thermodynamic explanation for this trend could come from order-of-magnitude comparisons for the pK_a of the species present in solution. The main equilibrium reactions that control speciation in a MEA/PZ/H₂O system include:



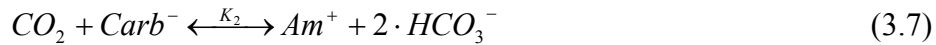
At low loading, the net chemical equilibrium reaction (derived by subtracting 3.2 from 3.3) is represented as:



$$K_1 = \frac{K_{carb}}{K_a} \quad (3.6)$$

The carbamate stability constants (K_{carb}) of free MEA and PZ, which are primarily available at low loading, were assumed be of the same order of magnitude as confirmed by measurements performed by Sartori and Savage (1983) for MEA and Cullinane (2005) for PZ. However, the pK_a of MEA at 40 and 60 °C at 9.1 and 9.7, respectively (Jou *et al.*, 1995) is markedly different from the average pK_a of PZ under the same conditions. Hetzer et al. (1968) report the pK_a of the first and second dissociation of piperazinium ion at 25 °C. Extrapolation to 40 and 60 °C yield 5.1 and 4.8 for the first dissociation and 9.4 and 8.9 for the second dissociation. Since 7m MEA/2m PZ has a lower average pK_a , it follows from Equation 3.6 that it also has a smaller equilibrium constant and therefore, will exhibit generally lower equilibrium partial pressures than the baseline 7m MEA as seen in Figure 3.2 for low loading.

Similarly, at high loading, the net chemical equilibrium reaction (derived from subtracting 3.2 and 3.3 from 2 times 3.4) is given by



$$K_2 = \frac{K_{a,co_2}}{K_a \cdot K_{carb}} \quad (3.8)$$

At higher loading, the average pK_a of PZ is about the same as the pK_a of MEA at both 40 and 60 °C. This is mainly because of the absence of piperazinium ion at higher loadings and the appearance of H^+PZCOO^- which has a pK_a comparable to MEA. However, the

stability constant of PZCOO^- is about six times less than PZ or MEA (Cullinane, 2005). Thus, it can be seen from Equation 3.8 that the equilibrium constant and equilibrium partial pressures of 7m MEA/2m PZ will be less than 7m MEA at high loading at the same temperatures.

Furthermore, Figure 3.2 shows the predicted VLE for 5.6m MEA/1.8m PZ is generally lower at 40 °C as compared 60 °C, under the same conditions. An increase of the total amine and total piperazine concentration to 7m MEA/2m PZ shows depressed partial pressures at 40 °C for high loading and virtually no change at low loading. However, elevated partial pressures are generally observed at 60 °C.

Solvent capacities, defined as moles of carbon dioxide in one kilogram of water, were calculated from Figure 3.2 between 500 and 10,000 Pa for 7m MEA/2m PZ, 5.6m MEA/1.8m PZ, and 7m MEA as 2.2, 1.4, and 0.7 mol $\text{CO}_2/\text{kg H}_2\text{O}$, respectively at 60 °C. In other words, 7m MEA/2m PZ capacity is a factor of three greater than 7m MEA and a factor of two greater than 5.6m MEA/1.8m PZ in the 0.5-10 kPa equilibrium partial pressure range.

3.3. Absorption Rate of CO_2 in 7m MEA/2m PZ

The absorption rate of CO_2 , given as a normalized flux (Section 2.5.1), into 7m MEA/2m PZ is compared to literature values for 7m MEA and several amine blends including 5.6m MEA/1.8m PZ, 7m MEA and 5m K^+ /2.5m PZ, and 14m DGA/3.5m MOR at 40 and 60 °C in Figures 3.3 and 3.4.

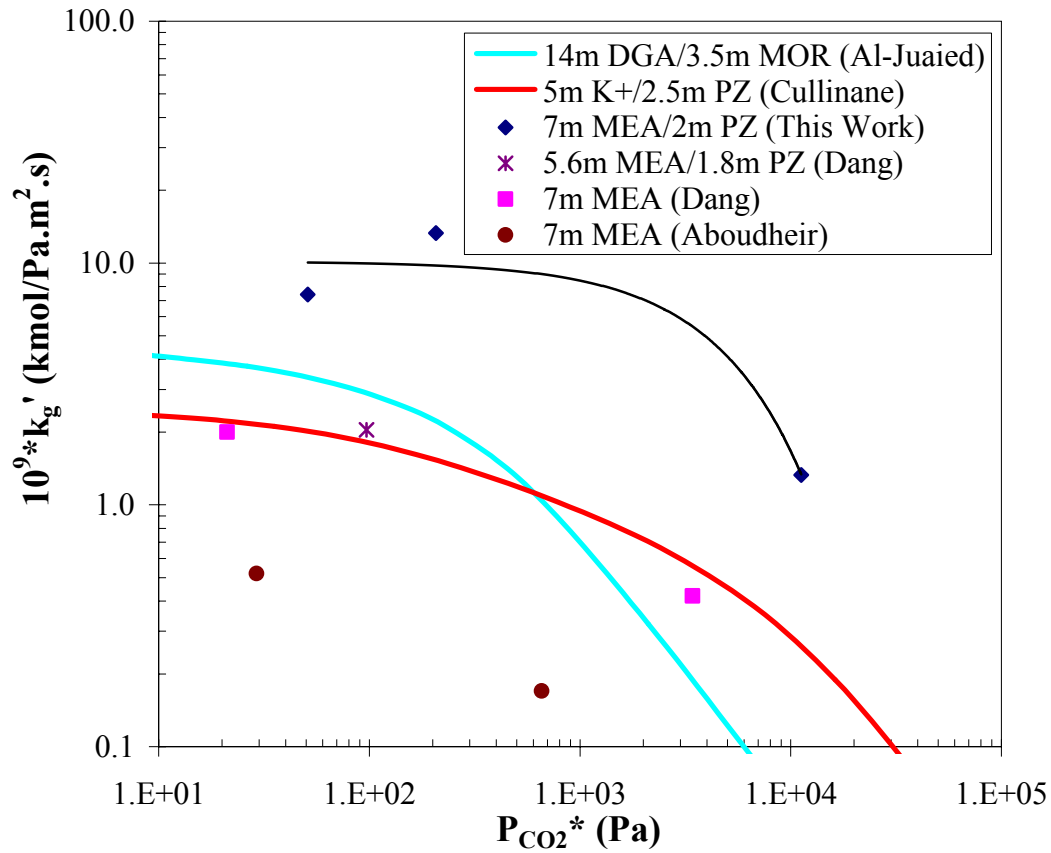


Figure 3.3 CO₂ Absorption in MEA/PZ blends at 40 °C

Figure 3.3 shows that absorption rate in 7m MEA/2m PZ is 3-5 times that of 5m K⁺/2.5m PZ and 7m MEA at 40 °C while Figure 3.4 shows that absorption rate in 7m MEA/2m PZ is 3-6 times that of 5m K⁺/2.5m PZ and 7m MEA at 60 °C. Rate data gathered by Dang (2001) for 5.6m MEA/1.8m PZ suggest absorption rates that are 1.5-2 times greater than baseline 7m MEA; hence, 2-3 times smaller than the absorption rates in 7m MEA/2m PZ. This phenomenon can be explained primarily by the fact that the latter solvent contains a higher total amine and total piperazine concentration than Dang's 5.6m MEA/1.8m PZ. Both figures show that absorption rate in 7m MEA/2m PZ decreases sharply as $P_{CO_2}^*$ increases, as expected due to consumption of the reactive amine.

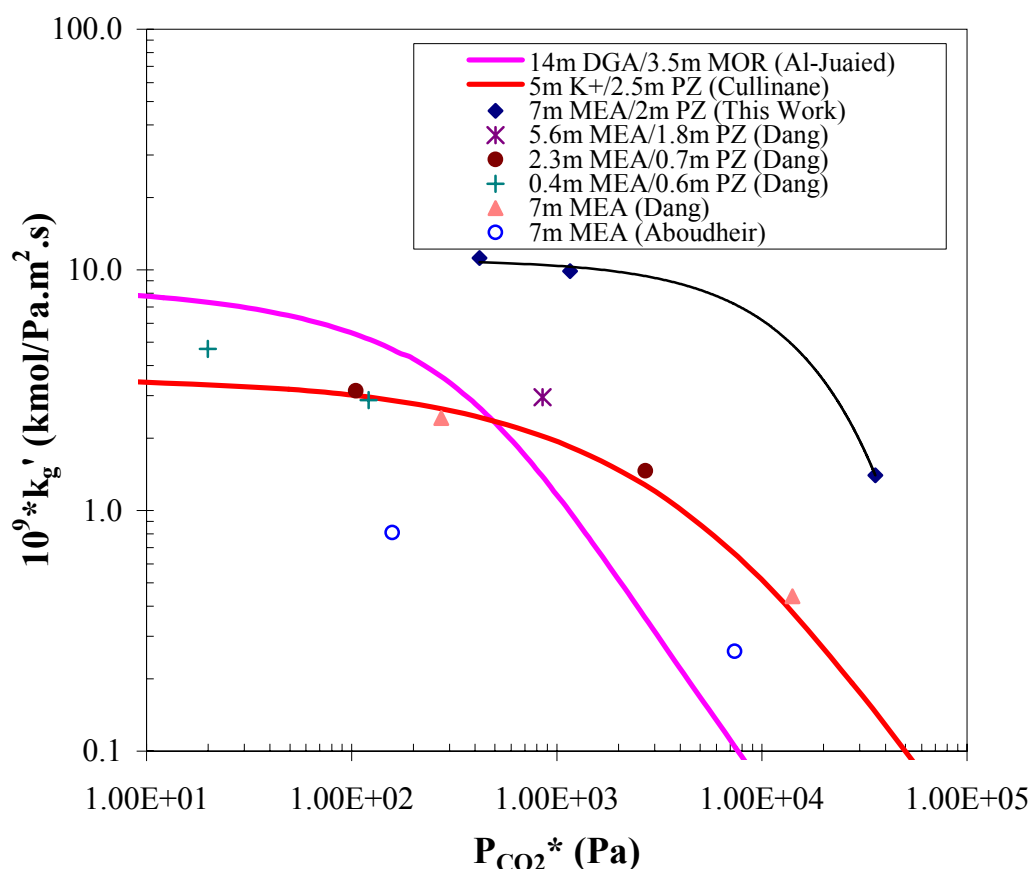


Figure 3.4 CO₂ Absorption in MEA/PZ blends at 60 °C

Rate data for 14m Diglycolamine®/3.5m Morpholine is also compared at both temperatures. At 40 °C, 14m DGA/3.5m MOR is 1.5-2 faster than 5m K⁺/2.5m PZ at partial pressures less than about 1 kPa and 2-3 times slower for partial pressures greater than 1 kPa. The rates are faster at 60 °C. 14m DGA/3.5m MOR is 2-3 faster than 5m K⁺/2.5m PZ at partial pressures less than about 1 kPa and 4-5 slower for partial pressures greater than 1 kPa. Nonetheless, the rates in 7m MEA/2m PZ surpass those in 14m DGA/3.5m MOR at both temperatures.

Aboudheir (2005) also predicted the apparent rate constant k_1 , for the absorption of CO_2 for loaded 7m MEA using a kinetics model. These values, in conjunction with diffusivity of CO_2 in MEA and Henry's constant for the absorption of CO_2 which were determined via N_2O analogy as described in Section 2.3.3 were used to calculate the normalized flux, k_g' , as follows:

$$k_g' = \frac{\sqrt{k_1 D_{\text{CO}_2}}}{H_{\text{CO}_2}} \quad (3.9)$$

The calculated normalized fluxes for 7m MEA as a function of CO_2 partial pressure at 40 and 60 °C are presented in Figures 3.3 and 3.4, respectively. The absorption rates differ from Dang (2001) absorption data for 7m MEA by approximately an order of magnitude. This discrepancy might be explained by inherent errors involved in calculating k_1 (15-20%), D_{CO_2} (10%), and H_{CO_2} (10%).

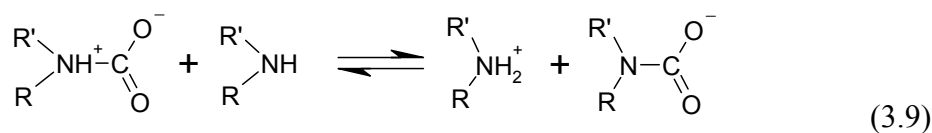
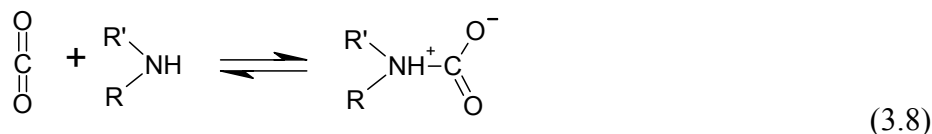
The increased absorption rate observed with the addition of piperazine to MEA can be explained by several reasons. First, the reaction rate of piperazine with CO_2 is very fast as evidenced by its overall rate constants. Table 3.2 summarizes the rate constants for some relevant amines. Piperazine has a greater rate constant than MEA, DGA, and Morpholine. Therefore, the presence of piperazine in aqueous solvent blends will accelerate its CO_2 absorption rate as observed in Figure 3.4. Figure 3.4 shows increase in rate with increasing PZ concentration. In other words, the rate increases from 0.4m MEA/0.6m PZ, to 2.3m MEA/0.7m PZ, to 5.6m MEA/1.8m PZ, and finally to 7m MEA/2m PZ. Furthermore, the piperazine appears more effective in promoting absorption in MEA than morpholine (another cyclic amine) promotes in DGA because of the relative magnitude of its overall rate constant. Second, a large concentration of MEA

Table 3.2 Overall Rate Constants for 1.0 M Amines at 25°C (Cullinane, 2005)

Amine	Source ^a (Rate/pK _a)	pK _a	Rate Constant ^b (s ⁻¹)	ΔH _r (kJ/mol)
Piperazine	9/9	9.73	102.2×10 ³	35.0
Monoethanolamine	1/2	9.55	5.9×10 ³	41.2
Diethanolamine	1/2	8.88	1.3×10 ³	53.1
Diglycolamine	3/4	9.46	4.52×10 ³	39.4
	5/4		6.7×10 ³	40.1
Ethylenediamine	6/2	9.91	15.1×10 ³	-
Piperidine	7/2	11.12	93.3×10 ³	-
	8/2		60.3×10 ³	-
Morpholine	3/2	8.49	20.6×10 ³	-
	7/2		20.0×10 ³	-
	5/2		22.3×10 ³	23.3

- a. 1. Hikita *et al.* (1977). 2. Perrin *et al.* (1981). 3. Alper (1990a). 4. Littel *et al.* (1990a). 5. Al-Juaied (2004). 6. Jensen and Christensen (1955). 7. Sharma (1965). 8. Jensen *et al.* (1952). 9. Cullinane (2005)
- b. Overall rate constant ($k = k_{Am} [Am]$ or $k_{Am-Am} [Am]^2 + k'_{Am-H_2O} [Am]$) assuming 25°C, negligible loading, and negligible hydroxide contributions.

will catalyze PZ, in a similar fashion as carbonate and hydroxyl ions, by extracting protons from the intermediate PZ molecule as described by the Caplow (1968) zwitterion mechanism (Equations 3.8 and 3.9).



Lastly, for loaded solutions, more concentrated amines possess a greater ionic strength, hence greater propensity to act as a base.

Chapter 4 : Conclusions and Recommendations

4.1. Conclusions

The absorption rate of CO₂ in 7m MEA/2m PZ is the fastest amongst all solvents compared in this work. It is 2-3 times faster than 5.6m MEA/1.8m PZ at both 40 and 60 °C, 3-5 times faster than 7m MEA and 5m K⁺/2.5m PZ at 40 °C and 3-6 times faster than 7m MEA and 5m K⁺/2.5m PZ at 60 °C. In addition, for partial pressures less than 1 kPa, the absorption rate of CO₂ in 7m MEA/2m PZ is 2 times greater than 14m DGA/3.5m MOR and 7-8 times greater for CO₂ partial pressures less than 1 kPa. Piperazine therefore is a very effective promoter of monoethanolamine.

The general trend for the equilibrium partial pressure of CO₂ in 7m MEA/2m PZ is that at low loading ($\alpha < 0.5$), $P_{\text{CO}_2}^*$ is elevated when compared to 7m MEA at both 40 and 60 °C. On the other hand, at higher loading ($\alpha > 0.5$), there appears to be a slight depression in $P_{\text{CO}_2}^*$ for 7m MEA/2m PZ when compared to 7m MEA. The solvent capacity of 7m MEA is tripled upon the addition of 2m PZ to give the 7m MEA/2m PZ solvent.

4.2. Recommendations

A rigorous thermodynamic model such as a standalone electrolyte NRTL VLE model should be developed using the VLE data for 7m MEA/2m PZ contained in this work and previous data reported by Dang (2001). Such a model will assist in the

prediction of speciation and solvent capacity through the regression of model parameters in the rigorous MEA/PZ VLE model for this system. As a guide, similar models for MEA and $\text{K}_2\text{CO}_3/\text{PZ}$ are available. Further, a rigorous VLE model will make for the extraction of more accurate kinetic information from, say, a rate model developed for the absorption of CO_2 in MEA/PZ/ H_2O .

More rigorous approaches are also needed for the rate model for CO_2 absorption in MEA/PZ/ H_2O . One of them is the partial differential equation method based on penetration theory. Bishnoi and Rochelle (2000) have developed a PDE rate model for MDEA/PZ/ H_2O system. Similar work could be done for MEA/PZ/ H_2O in the future.

VLE measurement of speciation of loaded amine solution with nuclear magnetic resonance can be an effective method for verifying VLE models. A suitable chemical shift reference such as a few drops of 2,2-dimethyl-2-silapentane-5-sulfonic acid (DSS) in D_2O can be used in an attempt to eliminate peak overlap in especially in ^{13}C spectrum for partially loaded MEA/PZ blends.

Appendix A : ^1H and ^{13}C NMR Spectra

This appendix archives the ^1H and ^{13}C NMR spectra that were used to develop data presented in Section 2.2. The first batch of spectra was obtained for 7m MEA while the second batch was obtained for 7m MEA/2m PZ.

MEA/D2O
Temp = 27C
Pulse Sequence: s2pu1

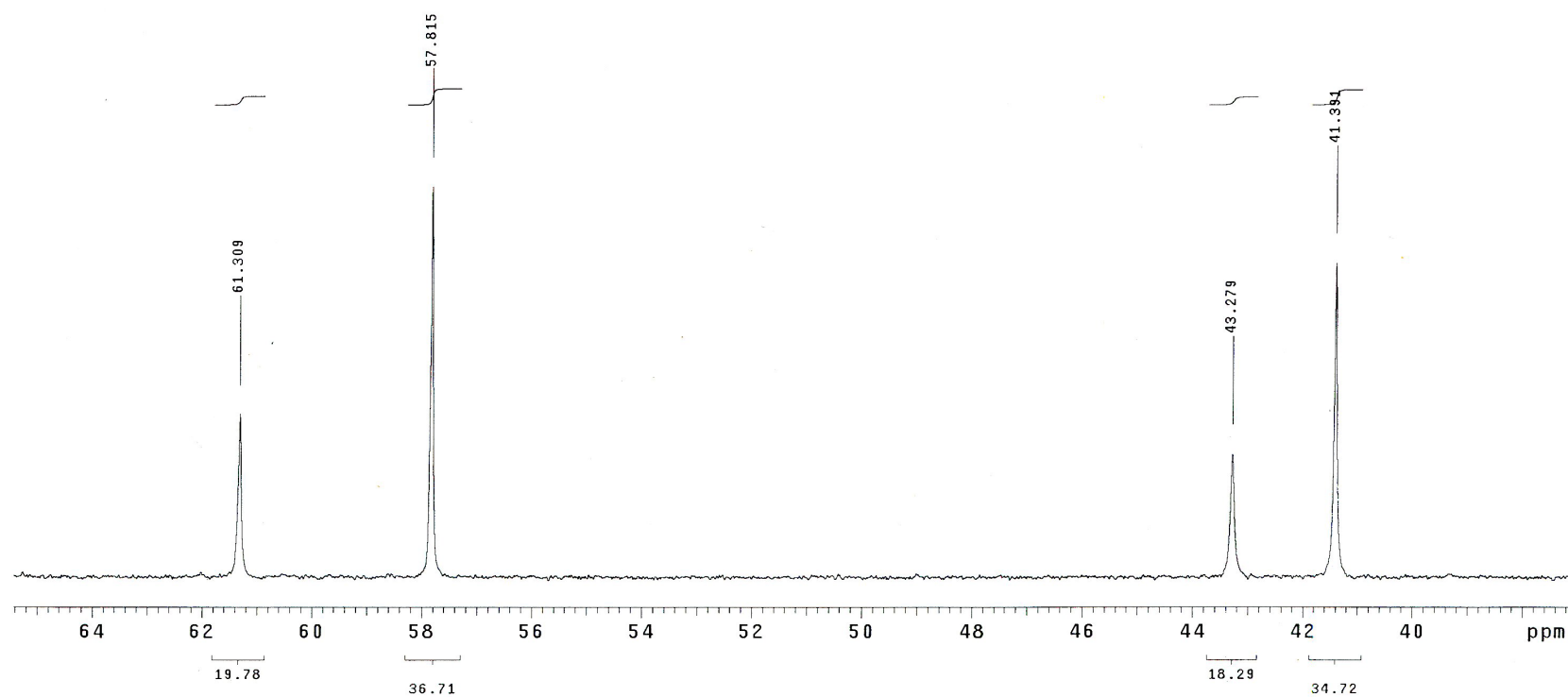


Figure A. 1 ^{13}C NMR Spectrum (Low End) of 7m MEA, $\alpha = 0.57$, $T = 27^\circ\text{C}$

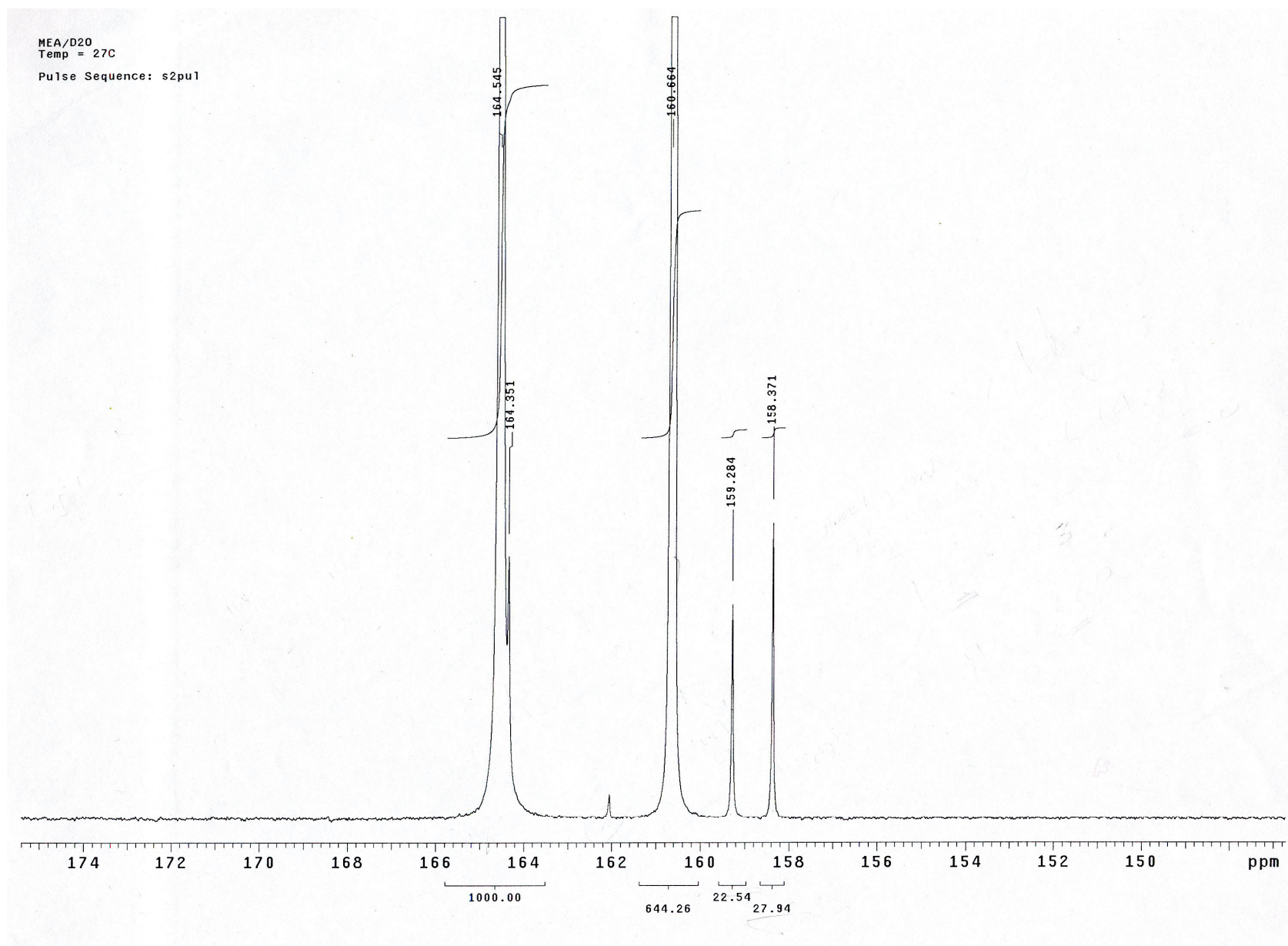


Figure A. 2 ^{13}C NMR Spectrum (High End) of 7m MEA, $\alpha = 0.57$, $T = 27\text{ }^{\circ}\text{C}$

MEA D2O Co2

exp6 gHSQC

SAMPLE		FLAGS	ACQUISITION		ARRAYS
date	Jun 17 2004	hs	n	array	phase
solvent	D2O	sspul	y	arraydim	256
sample	undefined	PFGflg	y		
ACQUISITION		hsglv1	4694	i	phase
sw	4001.6	SPECIAL	1	1	
at	0.128	temp	27.0	2	2
np	1024	gain	30		
fb	not used	spin	0		
ss	8	GRADIENTS			
d1	2.000	gzlv11	4694		
nt	4	gt1	0.002000		
2D ACQUISITION		gzlv13	2354		
sw1	25141.4	gt3	0.001000		
ni	128	gstab	0.000500		
phase	arrayed	F2 PROCESSING			
TRANSMITTER		gf	0.059		
tn	H1	gfs	not used		
sfrq	499.868	fn	1024		
tof	-171.4	F1 PROCESSING			
tpwr	57	gfl	0.009		
pw	11.000	gfs1	not used		
DECOUPLER		proc1	lp		
dn	C13	fn1	2048		
dof	-1258.5	DISPLAY			
dm	nnv	sp	1218.2		
dmm	cng	wp	500.2		
dmf	14285	sp1	4300.2		
dpwr	40	wp1	4517.6		
pxlv1	56	rfl	-327.2		
pxw	9.500	rfp	0		
HSQC		rfl1	1887.0		
j1xh	140.0	rflp1	0		
nullflg	y	PLOT			
mult	2	wc	115.8		
		sc	10.0		
		wc2	115.8		
		sc2	0		
		vs	986		
		th	2		
		al	cdc ph		

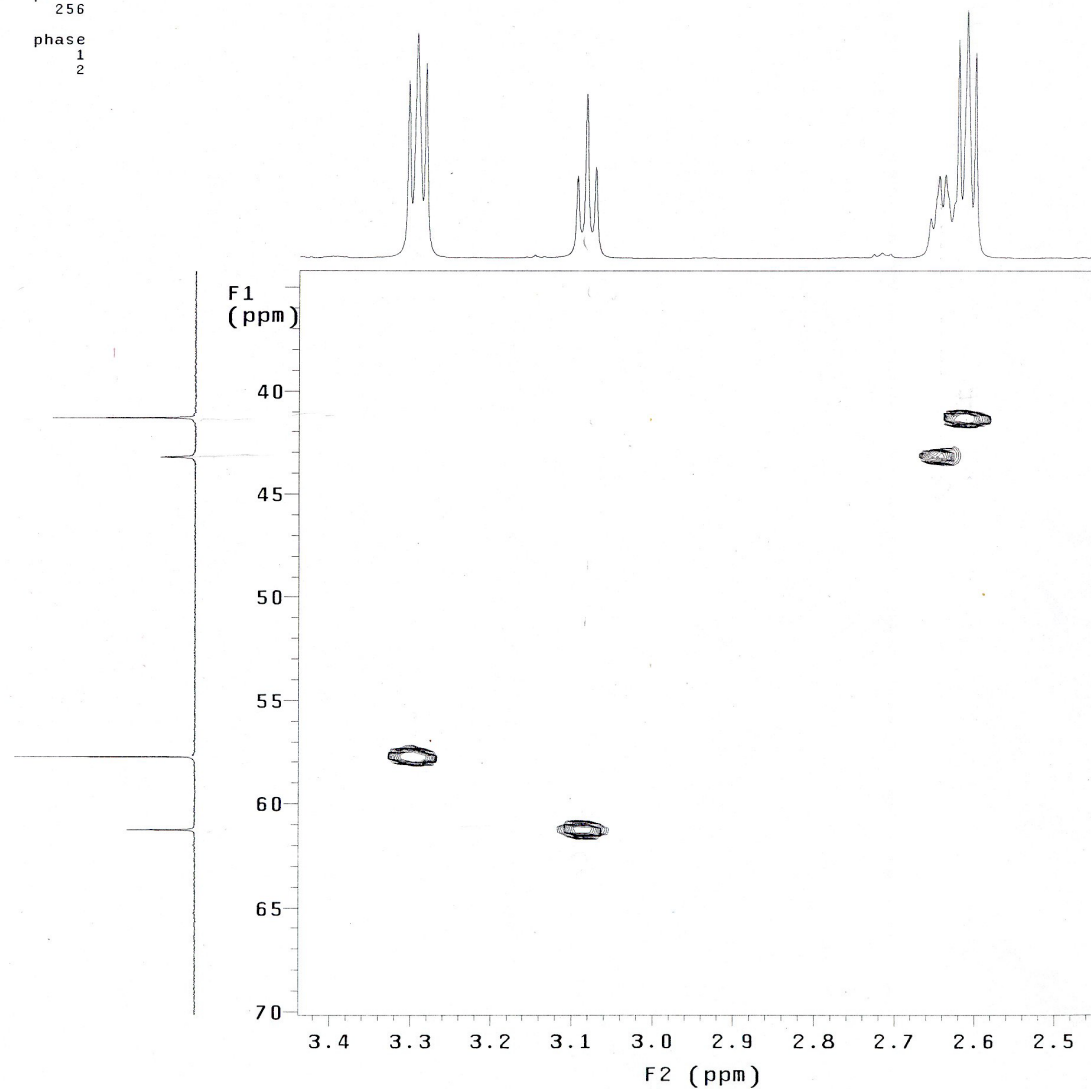


Figure A. 3 Combined ^1H and ^{13}C NMR Spectrum of 7m MEA, $\alpha = 0.57$, $T = 27^\circ\text{C}$

0902-MEAP225

Pulse Sequence: s2pu1

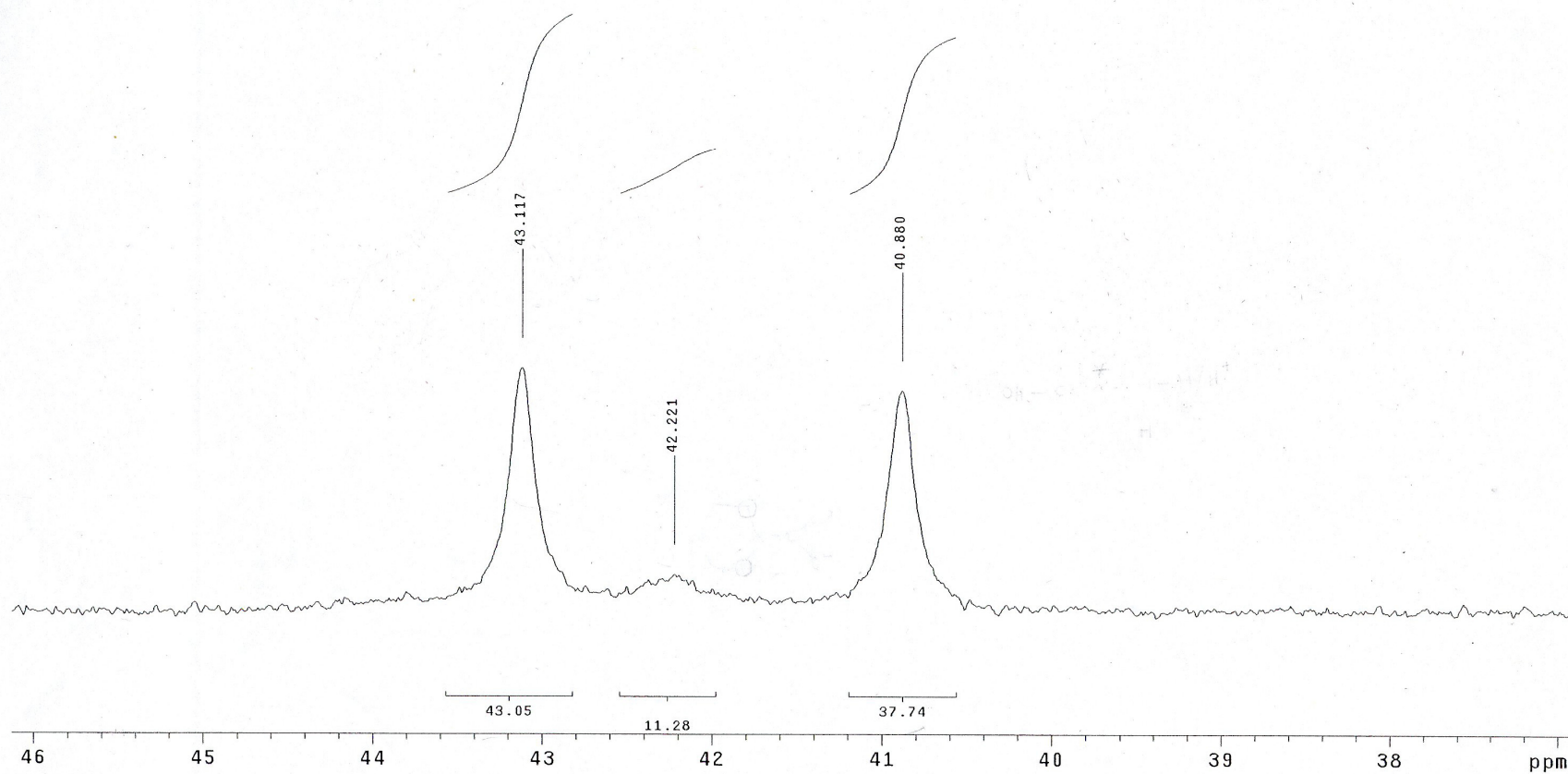


Figure A. 4 ^{13}C NMR Spectrum (Low End) of 7m MEA/2m PZ, $\alpha = 0.30$, $T = 27\text{ }^{\circ}\text{C}$

0902-MEAP225

Pulse Sequence: s2pu1

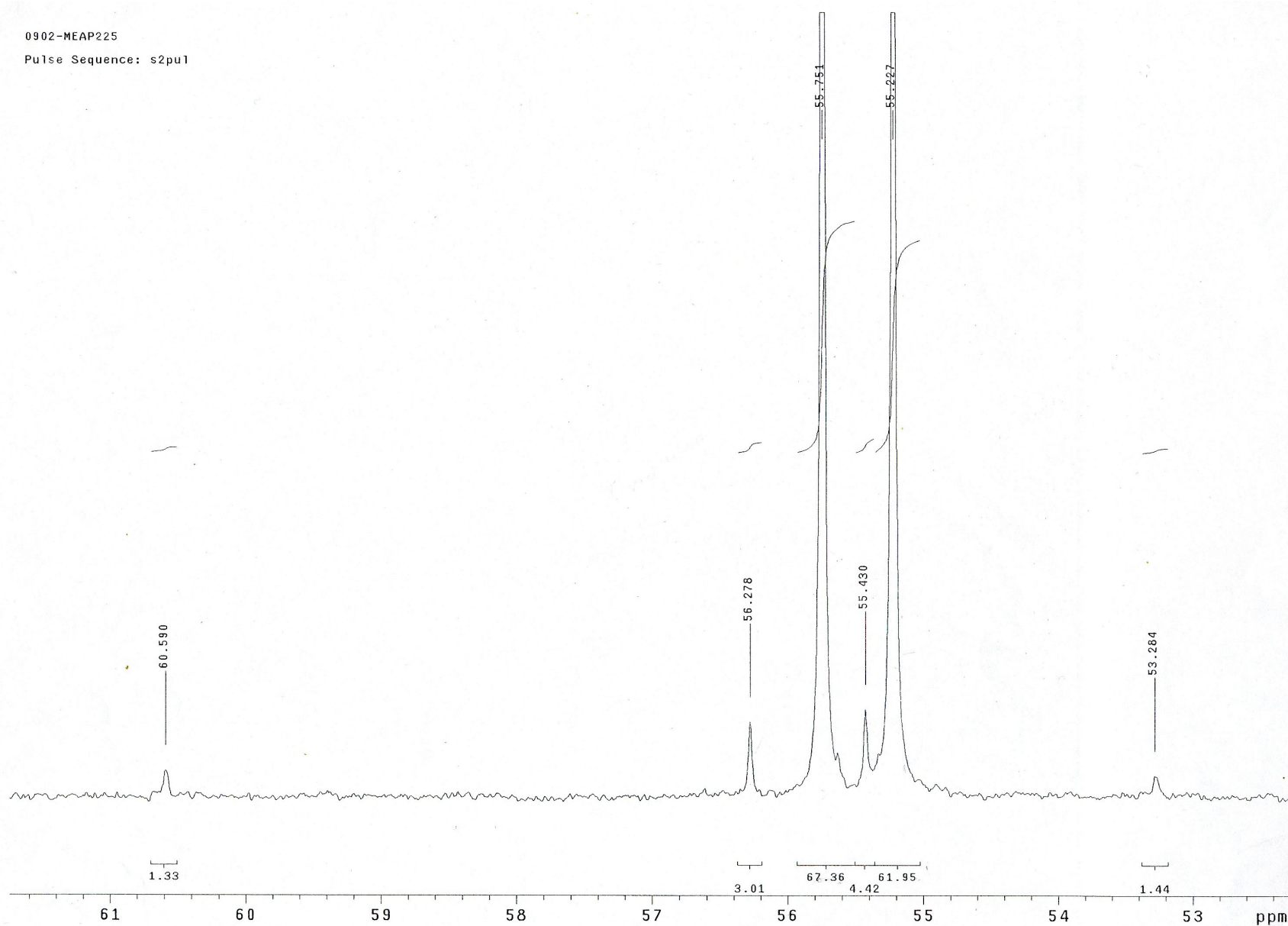


Figure A. 5 ^{13}C NMR Spectrum (Intermediate) of 7m MEA/2m PZ, $\alpha = 0.30$, $T = 27^\circ\text{C}$

0902-MEAP225

Pulse Sequence: s2pu1

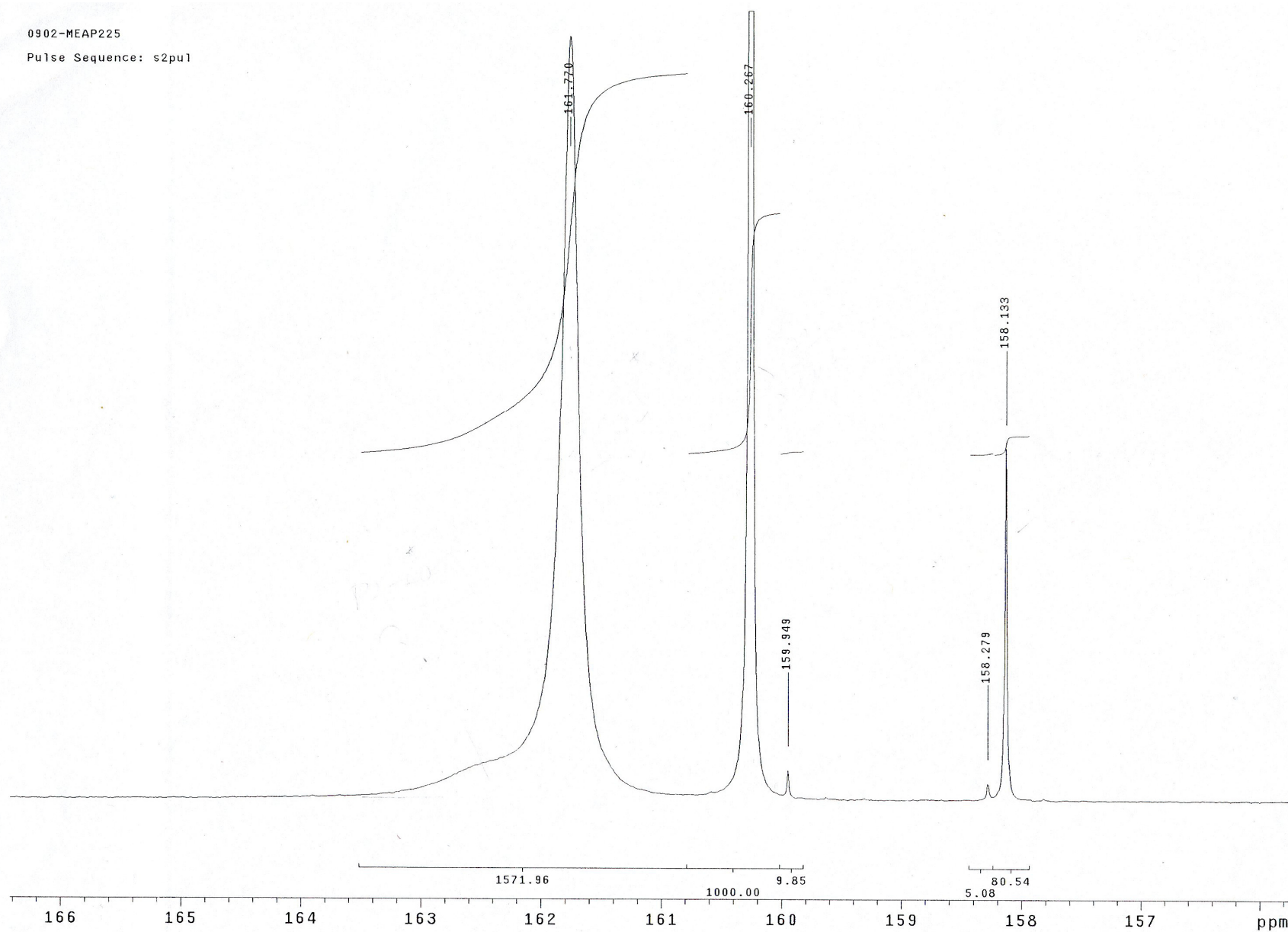


Figure A. 6 ^{13}C NMR Spectrum (High End) of 7m MEA/2m PZ, $\alpha = 0.30$, $T = 27^\circ\text{C}$

0902-MEAP225

Pulse Sequence: gHSQC

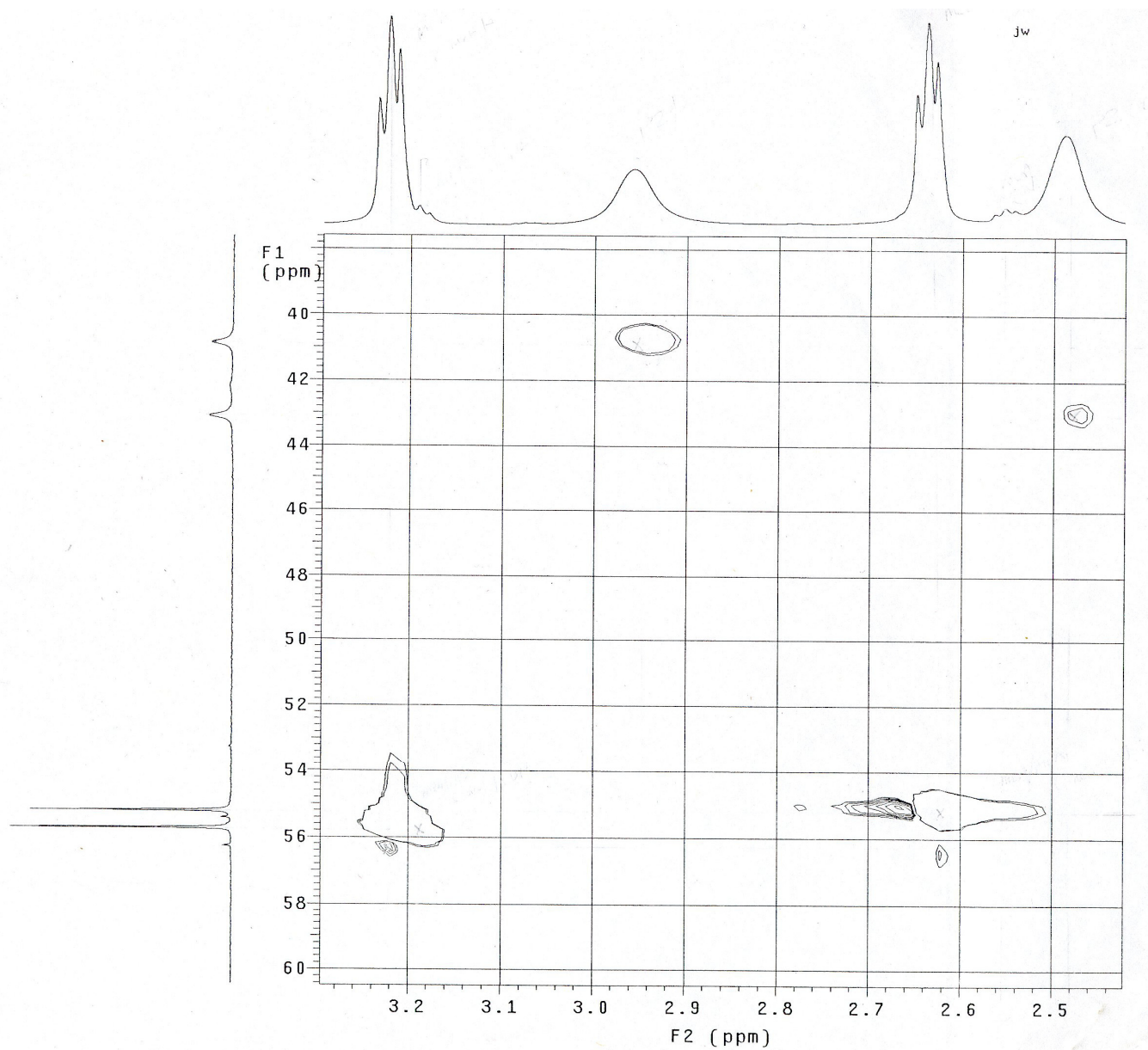


Figure A. 7 ^1H and ^{13}C NMR Spectrum of 7m MEA/2m PZ, $\alpha = 0.30$, $T = 27^\circ\text{C}$

0902-MEAP225

Pulse Sequence: s2pu1

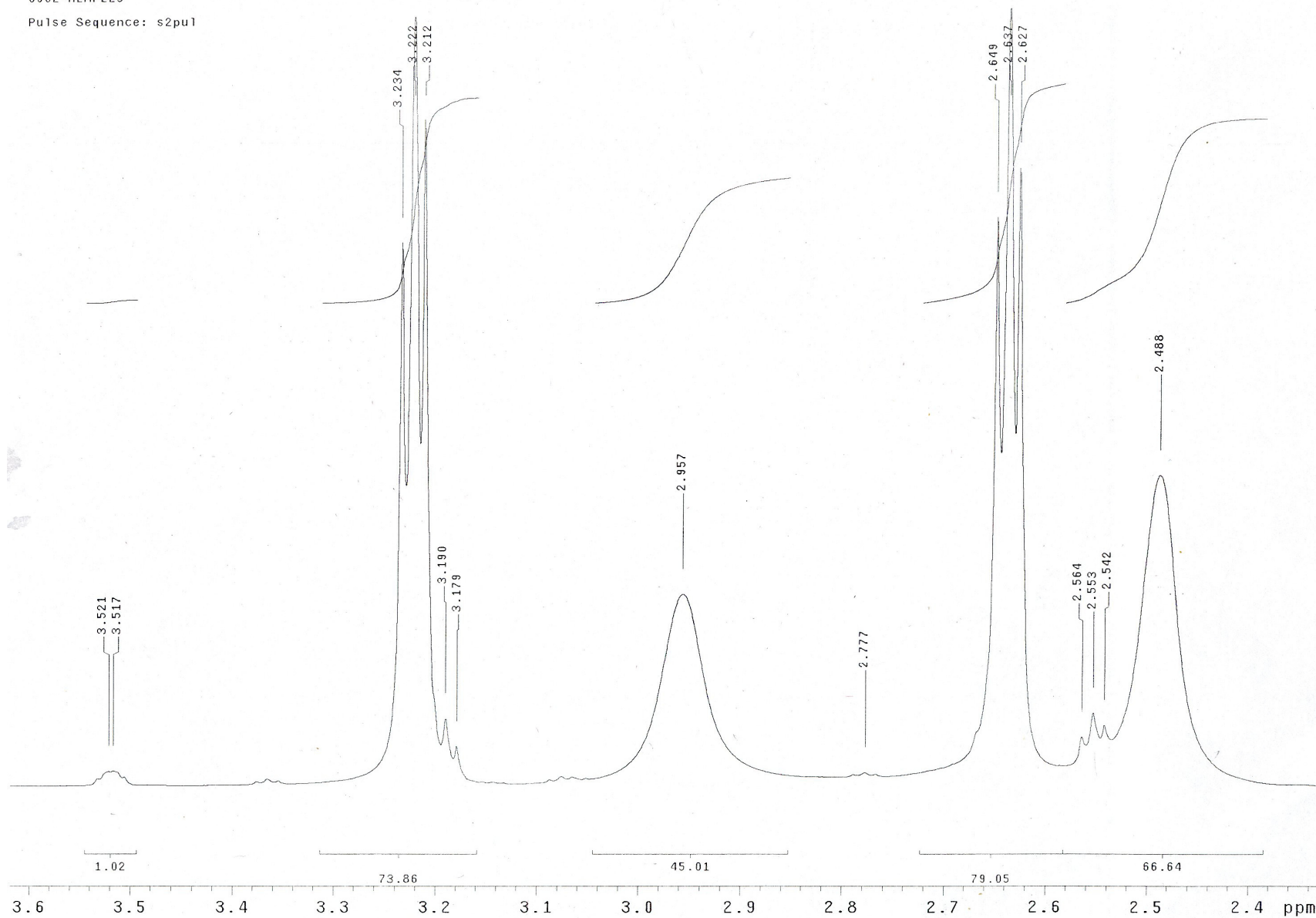


Figure A. 8 ^1H NMR Spectrum of 7m MEA/2m PZ, $\alpha = 0.30$, $T = 27\text{ }^\circ\text{C}$

Appendix B : Detailed Results

Detailed information concerning each wetted-wall column experiment performed in this work is presented. The solvents of interest are 7m MEA/2m PZ and 7m MEA. The associated concentrations and equilibrium partial pressure identify each data set.

The last three parameters in each table estimate the potential error associated with the results of each experimental point. The percent gas transfer resistance, K_G/k_g , represents the amount of mass transfer resistance attributable to the gas phase. A value greater than 50% indicates that much of the resistance lies in the gas phase diffusion of CO_2 to the interface. An approach to equilibrium, $(P_{\text{CO}_2,i} - P_{\text{CO}_2}^*)/P_{\text{CO}_2,i}$, measures the proximity of a data point to equilibrium. Therefore, approach values very close to zero indicate points very close to equilibrium. These are generally not used in determining rates. Finally, CO_2 absorption describes the sensitivity associated with flux measurement. Low CO_2 absorption or removal decreases the accuracy of flux measurements.

Table B. 1 7m MEA/2m PZ, $\alpha = 0.28$, T = 40 °C, $P_{CO_2}^* = 51$ Pa

Sample	1	2	3	4	5	6
Flux (kmol/m ² -s)	6.56E-07	1.08E-06	2.95E-06	5.33E-06	6.50E-06	7.98E-06
K _G (kmol/Pa-m ² -s)	3.20E-09	2.17E-09	2.17E-09	2.02E-09	2.04E-09	2.16E-09
kg (kmol/(Pa-m ² -s))	3.38E-09	3.38E-09	3.38E-09	3.39E-09	3.40E-09	3.40E-09
k _l ⁰ (cm/sec)	5.21E-03	5.21E-03	5.21E-03	5.22E-03	5.22E-03	5.22E-03
P _{CO₂b} (Pa)	255	550	1410	2682	3230	3752
P _{CO₂i} (Pa)	61	229	538	1113	1317	1407
P _{CO₂} [*] (Pa)	51	51	51	51	51	51
H _{CO₂} (kPa-L/mole)	8.00E+03	8.00E+03	8.00E+03	8.00E+03	8.00E+03	8.00E+03
D _{CO₂} (cm ² /s)	7.62E-06	7.63E-06	7.63E-06	7.64E-06	7.64E-06	7.63E-06
K _G /k _g (%)	94.8	64.2	64.1	59.6	60.2	63.4
(P _{CO₂i} -P _{CO₂} [*])/P _{CO₂i}	0.175	0.780	0.906	0.955	0.962	0.964
CO ₂ Absorption (%)	28.5	21.9	23.2	21.9	22.2	23.4

Table B. 2 7m MEA/2m PZ, $\alpha = 0.37$, T = 40 °C, $P_{CO_2}^* = 207$ Pa

Sample	1	2	3	4	5	6
Flux (kmol/m ² -s)	1.67E-07	8.57E-07	2.56E-06	3.95E-06	5.44E-06	7.95E-06
K _G (kmol/Pa-m ² -s)	-6.42E-09	3.38E-09	3.37E-09	3.40E-09	2.95E-09	3.00E-09
kg (kmol/(Pa-m ² -s))	4.36E-09	4.36E-09	4.37E-09	4.36E-09	4.37E-09	4.38E-09
k _l ⁰ (cm/sec)	5.23E-03	5.24E-03	5.24E-03	5.23E-03	5.23E-03	5.23E-03
P _{CO₂b} (Pa)	181	461	967	1369	2050	2862
P _{CO₂i} (Pa)	142	264	380	463	805	1046
P _{CO₂} [*] (Pa)	207	207	207	207	207	207
H _{CO₂} (kPa-L/mole)	8.67E+03	8.67E+03	8.67E+03	8.67E+03	8.67E+03	8.67E+03
D _{CO₂} (cm ² /s)	7.82E-06	7.84E-06	7.84E-06	7.83E-06	7.83E-06	7.82E-06
K _G /k _g (%)	-147.1	77.4	77.2	77.9	67.5	68.4
(P _{CO₂i} -P _{CO₂} [*])/P _{CO₂i}	-0.452	0.217	0.456	0.553	0.743	0.802
CO ₂ Absorption (%)	7.7	15.5	22.0	23.9	22.0	22.9

Table B. 3 7m MEA/2m PZ, $\alpha = 0.57$, T = 40 °C, $P_{CO_2}^* = 11224$ Pa

Sample	1	2	3	4	5	6	7	8
Flux (kmol/m ² -s)	-2.98E-06	-6.13E-06	-8.33E-06	1.34E-05	1.27E-05	1.24E-05	1.67E-05	1.83E-05
K _G (kmol/Pa-m ² -s)	3.23E-10	1.43E-09	3.64E-09	1.28E-09	8.58E-10	6.47E-10	5.87E-10	5.21E-10
kg (kmol/(Pa-m ² -s))	1.44E-09	1.46E-09	1.47E-09	1.50E-09	1.52E-09	1.54E-09	1.58E-09	1.55E-09
k _l ⁰ (cm/sec)	5.32E-03	5.35E-03	5.35E-03	5.34E-03	5.33E-03	5.33E-03	5.33E-03	5.33E-03
P _{CO₂b} (Pa)	1977	6939	8937	21674	26054	30390	39589	46305
P _{CO₂i} (Pa)	4048	11135	14599	12784	17687	22338	29022	34487
P _{CO₂} [*] (Pa)	11224	11224	11224	11224	11224	11224	11224	11224
H _{CO₂} (kPa-L/mole)	1.00E+04	1.01E+04	1.01E+04	1.00E+04	1.00E+04	1.00E+04	1.00E+04	1.00E+04
D _{CO₂} (cm ² /s)	7.57E-06	7.63E-06	7.63E-06	7.61E-06	7.59E-06	7.59E-06	7.59E-06	7.59E-06
K _G /k _g (%)	22.4	97.9	247.5	85.1	56.4	42.0	37.3	33.7
(P _{CO₂i} -P _{CO₂} [*])/P _{CO₂i}	-1.773	-0.008	0.231	0.122	0.365	0.498	0.613	0.675
CO ₂ Absorption (%)	-45.6	-26.3	-27.6	17.6	13.7	11.3	11.3	10.8

Table B. 4 7m MEA/2m PZ, $\alpha = 0.29$, T = 60 °C, $P_{CO_2}^* = 421$ Pa

Sample	1	2	3	4	5	6
Flux (kmol/m ² -s)	-4.62E-07	9.25E-07	2.62E-06	4.44E-06	5.62E-06	7.42E-06
K _G (kmol/Pa-m ² -s)	2.63E-09	2.56E-09	2.29E-09	2.35E-09	2.32E-09	2.37E-09
kg (kmol/(Pa-m ² -s))	3.53E-09	3.54E-09	3.55E-09	3.55E-09	3.56E-09	3.56E-09
k _l ⁰ (cm/sec)	6.01E-03	6.02E-03	6.02E-03	6.03E-03	6.03E-03	6.03E-03
P _{CO₂b} (Pa)	245	783	1567	2314	2844	3546
P _{CO₂i} (Pa)	376	522	828	1063	1264	1464
P _{CO₂} [*] (Pa)	421	421	421	421	421	421
H _{CO₂} (kPa-L/mole)	8.42E+03	8.42E+03	8.42E+03	8.42E+03	8.42E+03	8.42E+03
D _{CO₂} (cm ² /s)	9.89E-06	9.92E-06	9.92E-06	9.93E-06	9.93E-06	9.92E-06
K _G /k _g (%)	74.3	72.2	64.5	66.1	65.2	66.6
(P _{CO₂i} -P _{CO₂} [*])/P _{CO₂i}	-0.120	0.193	0.491	0.604	0.667	0.712
CO ₂ Absorption (%)	-20.1	12.6	17.8	20.3	20.9	22.1

Table B. 5 7m MEA/2m PZ, $\alpha = 0.40$, T = 60 °C, $P_{CO_2}^* = 1162$ Pa

Sample	1	2	3	4	5	6	7
Flux (kmol/m ² -s)	-3.39E-06	-2.32E-06	-9.05E-07	6.04E-07	2.82E-06	3.46E-06	4.92E-06
K _G (kmol/Pa-m ² -s)	3.43E-09	3.22E-09	3.86E-09	4.24E-09	3.56E-09	3.16E-09	3.16E-09
kg (kmol/(Pa-m ² -s))	4.57E-09	4.57E-09	4.58E-09	4.58E-09	4.59E-09	4.59E-09	4.60E-09
k _l ^O (cm/sec)	5.95E-03	5.94E-03	5.98E-03	5.97E-03	5.94E-03	5.93E-03	5.94E-03
P _{CO₂,b} (Pa)	174	442	927	1304	1955	2258	2720
P _{CO₂,i} (Pa)	916	950	1125	1172	1340	1504	1649
P _{CO₂}* (Pa)}	1162	1162	1162	1162	1162	1162	1162
H _{CO₂} (kPa-L/mole)	9.23E+03	9.23E+03	9.23E+03	9.23E+03	9.23E+03	9.24E+03	9.24E+03
D _{CO₂} (cm ² /s)	1.03E-05	1.02E-05	1.03E-05	1.02E-05	1.02E-05	1.03E-05	1.03E-05
K _G /k _g (%)	75.2	70.6	84.3	92.6	77.5	68.8	68.7
(P _{CO₂,i} -P _{CO₂}*)/P_{CO₂,i}}	-0.268	-0.223	-0.033	0.009	0.133	0.227	0.295
CO ₂ Absorption (%)	-155.4	-41.9	-7.8	3.7	11.4	12.2	14.3

Table B. 6 7m MEA/2m PZ, $\alpha = 0.57$, T = 60 °C, $P_{CO_2}^* = 35725$ Pa

Sample	1	2	3	4	5	6	7
Flux (kmol/m ² -s)	-8.62E-06	-4.77E-06	-9.71E-07	1.40E-05	2.12E-05	2.22E-05	2.77E-05
K _G (kmol/Pa-m ² -s)	6.63E-10	7.82E-10	-4.59E-10	7.74E-10	8.84E-10	7.46E-10	7.83E-10
kg (kmol/(Pa-m ² -s))	1.94E-09	1.98E-09	1.99E-09	2.12E-09	2.10E-09	2.08E-09	2.15E-09
k _l ^O (cm/sec)	6.17E-03	6.17E-03	6.20E-03	6.17E-03	6.20E-03	6.18E-03	6.19E-03
P _{CO₂,b} (Pa)	22714	29626	37841	53879	59662	65469	71052
P _{CO₂,i} (Pa)	27166	32040	38328	47239	49611	54783	58180
P _{CO₂}* (Pa)}	35725	35725	35725	35725	35725	35725	35725
H _{CO₂} (kPa-L/mole)	1.05E+04	1.05E+04	1.05E+04	1.05E+04	1.05E+04	1.05E+04	1.05E+04
D _{CO₂} (cm ² /s)	1.00E-05	1.00E-05	1.01E-05	1.00E-05	1.01E-05	1.01E-05	1.01E-05
K _G /k _g (%)	34.2	39.6	-23.0	36.6	42.0	35.9	36.4
(P _{CO₂,i} -P _{CO₂}*)/P_{CO₂,i}}	-0.315	-0.115	0.068	0.244	0.280	0.348	0.386
CO ₂ Absorption (%)	-8.3	-3.4	-0.5	5.1	6.9	6.7	7.4

Table B. 7 7m MEA, $\alpha = 0.35$, T = 60 °C, $P_{CO_2}^* = 212$ Pa

Sample	1	2	3	4	5	6
Flux (kmol/m ² -s)	-5.08E-07	3.05E-08	3.74E-06	8.42E-06	8.73E-06	1.45E-05
K _G (kmol/Pa-m ² -s)	-6.70E-09	7.90E-11	2.23E-09	2.62E-09	2.27E-09	2.65E-09
kg (kmol/(Pa-m ² -s))	3.45E-09	3.46E-09	3.47E-09	3.48E-09	3.48E-09	3.49E-09
k _l ⁰ (cm/sec)	8.06E-03	8.06E-03	8.07E-03	8.07E-03	8.06E-03	8.06E-03
P _{CO₂b} (Pa)	288	599	1888	3429	4054	5679
P _{CO₂i} (Pa)	435	590	809	1005	1545	1525
P _{CO₂} [*] (Pa)	212	212	212	212	212	212
H _{CO₂} (kPa-L/mole)	1.11E+04	1.11E+04	1.11E+04	1.11E+04	1.11E+04	1.11E+04
D _{CO₂} (cm ² /s)	1.30E-05	1.31E-05	1.31E-05	1.31E-05	1.31E-05	1.31E-05
K _G /k _g (%)	-193.9	2.3	64.4	75.4	65.3	76.0
(P _{CO₂i} -P _{CO₂} [*])/P _{CO₂i}	0.512	0.640	0.737	0.789	0.863	0.861
CO ₂ Absorption (%)	-18.8	0.5	21.0	25.9	22.7	26.8

Table B. 8 7m MEA, $\alpha = 0.43$, T = 60 °C, $P_{CO_2}^* = 8178$ Pa

Sample	1	2	3	4	5	6	7	8
Flux (kmol/m ² -s)	-5.97E-06	-3.51E-06	-2.41E-06	1.84E-07	3.20E-06	1.17E-05	1.27E-05	1.47E-05
K _G (kmol/Pa-m ² -s)	9.53E-10	7.43E-10	8.29E-10	2.70E-10	9.65E-10	1.39E-09	1.29E-09	1.39E-09
kg (kmol/(Pa-m ² -s))	4.52E-09	4.54E-09	4.56E-09	4.61E-09	4.64E-09	4.70E-09	4.72E-09	4.74E-09
k _l ⁰ (cm/sec)	7.46E-03	7.47E-03	7.47E-03	7.47E-03	7.47E-03	7.46E-03	7.47E-03	7.47E-03
P _{CO₂b} (Pa)	1920	3455	5277	8858	11490	16620	18015	18804
P _{CO₂i} (Pa)	3238	4227	5804	8818	10808	14124	15332	15690
P _{CO₂} [*] (Pa)	8178	8178	8178	8178	8178	8178	8178	8178
H _{CO₂} (kPa-L/mole)	1.19E+04	1.19E+04	1.19E+04	1.19E+04	1.19E+04	1.19E+04	1.19E+04	1.19E+04
D _{CO₂} (cm ² /s)	1.32E-05	1.32E-05	1.32E-05	1.32E-05	1.32E-05	1.32E-05	1.32E-05	1.32E-05
K _G /k _g (%)	21.1	16.3	18.2	5.9	20.8	29.6	27.3	29.3
(P _{CO₂i} -P _{CO₂} [*])/P _{CO₂i}	-1.526	-0.935	-0.409	0.073	0.243	0.421	0.467	0.479
CO ₂ Absorption (%)	-24.8	-8.1	-3.6	0.2	2.1	5.4	5.3	5.9

Nomenclature

a	Interfacial area of wetted wall column, (m^2)
$[C]$	Concentration, (mol/m^3)
d	Hydraulic diameter of the wetted wall column, (m)
D_x	Diffusion coefficient of x, (m^2/s)
H	Height of the wetted wall column, (m)
H	Henry's law constant, ($\text{kPa}\cdot\text{L}/\text{mol}$)
I	Ionic strength
K	Rate constant, ($1/\text{s}$)
k_g	Gas film mass transfer coefficient, ($\text{kmol}/(\text{Pa}\cdot\text{m}^2\cdot\text{s})$)
K_G	Overall mass transfer coefficient, ($\text{kmol}/(\text{Pa}\cdot\text{m}^2\cdot\text{s})$)
k_l°	Liquid film mass transfer coefficient, (m/s)
K	Equilibrium constant
M	Molecular weight
P_x	Partial pressure of x, (Pa)
Q_L	Flow rate, (m^3/s)
Re	Reynolds number
Sc	Schmidt number
Sh	Sherwood number
T	Temperature, (K)
V	Volume of solution, (m^3)
w	Mass percent of amine
X	Mole fraction
α	CO_2 loading, ($\text{mol CO}_2/\text{mol equivalent amine}$)
η	Parameter to calculate mass transfer coefficient
Θ	Parameter to calculate mass transfer coefficient

δ	Film thickness, (m)
τ	Contact time, (s)
μ	Viscosity, (Pa·s)
ρ	Density, (kg/m ³)

Bibliography

- U.S. EPA, (2004). *Inventory of U.S. Greenhouse Gas Emissions and Sinks: 1990-2002*. Washington, D.C.
- Aboudheir, A., P. Tontiwachwuthikul, A. Chakma and R. Idem (2003). Kinetics of the reactive absorption of carbon dioxide in high CO₂-loaded, concentrated aqueous monoethanolamine solutions. *Chem. Eng. Science* **58**: 5195-5210.
- Al-Ghawas, H. A., D. P. Hagewiesche, G. Ruiz-Ibanez and O. C. Sandall (1989). Physicochemical Properties Important for Carbon Dioxide Absorption in Aqueous Methyldiethanolamine. *J. Chem. Eng. Data* **34**(4): 385-391.
- Al-Juaied, M. (2004). Carbon Dioxide Removal from Natural Gas by Membranes in the Presence of Heavy Hydrocarbons and by Aqueous Diglycolamine®/Morpholine. Ph.D. Dissertation. The University of Texas at Austin.
- Amdur, I., J. W. Irvine, E. A. Mason and J. Ross (1952). Diffusion Coefficients of the Systems CO₂-CO₂ and CO₂-N₂O. *J. Chem. Phys.* **20**: 436-443.
- Austgen, D. M. (1989). A Model of Vapor-Liquid Equilibria for Acid Gas-Alkanolamine-Water Systems. Ph.D. Dissertation. The University of Texas at Austin.
- Bird, R. B., W. E. Stewart and E. N. Lightfoot (1960). Transport Phenomena. New York, Wiley.
- Bishnoi, S. (2000). Carbon Dioxide Absorption and Solution Equilibrium in Piperazine Activated Methyldiethanolamine. Ph.D. Dissertation. The University of Texas at Austin.
- Bishnoi, S. and G. T. Rochelle (2000). Absorption of Carbon Dioxide into Aqueous Piperazine: Reaction Kinetics, Mass Transfer and Solubility. *Chem. Eng. Sci.* **55**(22): 5531-5543.
- Bishnoi, S. and G. T. Rochelle (2002a). Absorption of Carbon Dioxide in Aqueous Piperazine/Methyldiethanolamine. *AIChE J.* **48**(12): 2788-2799.
- Bishnoi, S. and G. T. Rochelle (2002b). Thermodynamics of Piperazine/Methyldiethanolamine/ Water/Carbon Dioxide. *Ind. Eng. Chem. Res.* **41**(3): 604-612.

- Blauwhoff, P. M. M., G.F. Versteeg and W. P. M. V. Swaaij (1984). A Study on the Reaction between CO₂ and Alkanolamines in Aqueous Solutions. *Chem. Eng. Sci.* **39**(2): 207-225.
- Bosch, H., G. F. Versteeg and W. P. M. Van Swaaij (1990). Kinetics of the Reaction of Carbon Dioxide with the Sterically Hindered Amine 2-Amino-2-Methylpropanol at 298 K. *Chem. Eng. Sci.* **45**(5): 1167-1173.
- Bronsted, J. N. (1928). Acid and Basic Catalysis. *Chem. Rev.* **5**(3): 231-338.
- Browning, G. J. and R. H. Weiland (1994). Physical Solubility of Carbon Dioxide in Aqueous Alkanolamines Via Nitrous Oxide Analogy. *J. Chem. Eng. Data* **39**: 817-822.
- Cabani, S., G. Conti, D. Giannessi and L. Lepori (1975). Thermodynamic Study of Aqueous Dilute Solutions of Organic Compounds. 3. Morpholines and Piperazines. *J. Chem. Soc., Faraday Trans. 1* **71**(5): 1154-1160.
- Caplow, M. (1968). Kinetics of Carbamate Formation and Breakdown. *J. Am. Chem. Soc.* **90**(24): 6795-6803.
- Clarke, J. K. A. (1964). Kinetics of Absorption of Carbon Dioxide in Monoethanolamine Solutions at Short Contact Times. *Ind. Eng. Chem. Fund.* **3**(3): 239-245.
- Critchfield, J. E. (1988). CO₂ Absorption/Desorption in Methyldiethanolamine Solutions Promoted with Monoethanolamine and Diethanolamine: Mass Transfer and Reaction Kinetics. Ph.D. Dissertation. The University of Texas at Austin.
- Crooks, J. E. and J. P. Donnellan (1989). Kinetics and Mechanism of the Reaction between Carbon Dioxide and Amines in Aqueous Solution. *J. Chem. Soc., Perkin Trans. 2* **4**: 331-333.
- Crooks, J. E. and J. P. Donnellan (1990). Kinetics of the Reaction between Carbon Dioxide and Tertiary Amines. *J. Org. Chem.* **55**(4): 1372-1374.
- Cullinane, J. T. (2002). Carbon Dioxide Absorption in Aqueous Mixtures of Potassium Carbonate and Piperazine. M.S. Thesis. The University of Texas at Austin.
- Cullinane, J. T. and G. T. Rochelle (2004). Thermodynamics of Aqueous Potassium Carbonate, Piperazine, and CO₂ Mixtures. *Fluid Phase Equilib.* **227**(2): 197-213.

- Cullinane, J.T. (2005). Thermodynamics and Kinetics of Aqueous Piperazine with Potassium Carbonate for Carbon Dioxide Absorption. Ph.D. Dissertation. The University of Texas at Austin.
- Danckwerts, P. V. (1951). Significance of Liquid-Film Coefficients in Gas Absorption. *Ind. Eng. Chem.* **43**: 1460-1467.
- Danckwerts, P. V. and M. M. Sharma (1966). Absorption of Carbon Dioxide into Solutions of Alkalies and Amines. Hydrogen Sulfide and Carbonyl Sulfide. *Chemical Engineer (1904-20)* No. **202**: CE244-CE280.
- Danckwerts, P. V. (1979). The Reaction of Carbon Dioxide with Ethanolamines. *Chem. Eng. Sci.* **34**(4): 443-446.
- Dang, H. (2001). CO₂ Absorption Rate and Solubility in Monoethanolamine/Piperazine/Water. M.S. Thesis. The University of Texas at Austin.
- Ermatchkov, V., A. Perez-Salado Kamps and G. Maurer (2003). Chemical Equilibrium Constants for the Formation of Carbamates in (Carbon Dioxide + Piperazine + Water) from ¹H-NMR-Spectroscopy. *J. Chem. Thermodyn.* **35**(8): 1277-1289.
- Goel, S. (2005). Investigation of the Physical Solubility in Nitrous Oxide in Monoethanolamine/Piperazine Solvent. Senior Report. The University of Texas at Austin.
- Glasscock, D. and G. T. Rochelle (1989). Numerical Simulation of Theories for Gas Absorption with Chemical Reaction. *AIChE J.* **35**(8): 1271-1281.
- Glasscock, D. (1990). Modeling and Experimental Study of Carbon Dioxide Absorption into Aqueous Alkanolamines. The University of Texas at Austin.
- Hetzer, H. B., R. A. Robinson and R. G. Bates (1968). Dissociation Constants of Piperazinium Ion and Related Thermodynamic Quantities from 0 to 50°. *J. Phys. Chem.* **72**(6): 2081-2086.
- Hobler, T. (1966). Mass Transfer and Absorbers. Oxford, Pergamon Press.
- King, C. J. (1966). Turbulent Liquid-Phase Mass Transfer at a Free Gas-Liquid Interface. *Ind. Eng. Chem. Fund.* **5**(1): 1-8.
- Kohl, A. L. and F. C. Riesenfeld (1985). Gas Purification. Houston, Gulf Publishing.
- Laddha, S. S. and P. V. Danckwerts (1982). The Absorption of Carbon Dioxide by Amine-Potash Solutions. *Chem. Eng. Sci.* **37**(5): 665-667.

- Lewis, W. K. and W. G. Whitman (1924). Principles of Gas Absorption. *Ind. Eng. Chem.* **16**: 1215-1220.
- Lide, D. R., Ed. (2000). CRC Handbook of Chemistry and Physics. London, CRC Press.
- Littel, R. J., G. F. Versteeg and W. P. M. Van Swaaij (1992a). Kinetics of Carbon Dioxide with Primary and Secondary Amines in Aqueous Solutions. I. Zwitterion Deprotonation Kinetics for Dea and Dipa in Aqueous Blends of Alkanolamines. *Chem. Eng. Sci.* **47**(8): 2027-2035.
- Littel, R. J., G. F. Versteeg and W. P. M. Van Swaaij (1992b). Solubility and Diffusivity Data for the Absorption of COS, CO₂, and N₂O in Amine Solutions. *J. Chem. Eng. Data* **37**: 49-55.
- Littel, R. J., G. F. Versteeg and W. P. M. Van Swaaij (1992c). Kinetics of CO₂ with Primary and Secondary Amines in Aqueous Solutions--II. Influence of Temperature on Zwitterion Formation and Deprotonation Rates. *Chem. Eng. Sci.* **47**(8): 2037-2045.
- Mshewa, M. M. (1995). Carbon Dioxide Desorption/Absorption with Aqueous Mixtures of Methyldiethanolamine and Diethanolamine at 40 to 120°C. Ph.D. Dissertation. The University of Texas at Austin.
- Pacheco, M. A. (1998). Mass Transfer, Kinetics and Rate-Based Modeling of Reactive Absorption. Ph.D. Dissertation. The University of Texas at Austin.
- Pagano, J. M., D. E. Goldberg and W. C. Fernelius (1961). A Thermodynamic Study of Homopiperazine, Piperazine, and N-(2-Aminoethyl)Piperazine and Their Complexes with Copper(II) Ion. *J. Phys. Chem.* **65**: 1062-1064.
- Perrin, D. D., B. Dempsey and E. P. Serjeant (1981). pK_a Prediction for Organic Acids and Bases: 6-9, 36-37.
- Pigford, R. L. (1941). Counter-Diffusion in a Wetted-Wall Column. Ph.D. Dissertation. University of Illinois.
- Posey, M. L. (1996). Thermodynamic Model for Acid Gas Loaded Aqueous Alkanolamine Solutions. Ph.D. Dissertation. The University of Texas at Austin.
- Sartori, G. and D. W. Savage (1983). Sterically Hindered Amines for Carbon Dioxide Removal from Gases. *Ind. Eng. Chem. Fund.* **22**(2): 239-249.
- Savage, D. W., G. Sartori and G. Astarita (1984). Amines as Rate Promoters for Carbon Dioxide Hydrolysis. *Faraday Discuss. Chem. Soc.*(77): 17-31.

- Tamimi, A., E. B. Rinker and O. C. Sandall (1994a). Diffusivity of Nitrous Oxide in Aqueous Solutions of N-Methyldiethanolamine and Diethanolamine from 293 to 368 K. *J. Chem. Eng. Data* **39**(2): 396-398.
- Versteeg, G. F. (1987). Mass Transfer and Chemical Reaction Kinetics in Acid Gas Treating Processes. Ph.D. Dissertation. Twente University.
- Versteeg, G. F. and W. P. M. Van Swaaij (1988a). On the Kinetics between Carbon Dioxide and Alkanolamines Both in Aqueous and Non-Aqueous Solutions - II. Tertiary Amines. *Chem. Eng. Sci.* **43**(3): 587-591.
- Versteeg, G. F. and W. P. M. Van Swaaij (1988b). Solubility and Diffusivity of Acid Gases (CO_2 , N_2O) in Aqueous Alkanolamine Solutions. *J. Chem. Eng. Data* **33**(1): 29-34.
- Versteeg, G. F. and M. H. Oyevaar (1989). The Reaction between Carbon Dioxide and Diethanolamine at 298 K. *Chem. Eng. Sci.* **44**(5): 1264-1268.
- Versteeg, G. F., L. A. J. Van Duck and W. P. M. Van Swaaij (1996). On the Kinetics between CO_2 and Alkanolamines Both in Aqueous and Nonaqueous Solutions. An Overview. *Chem. Eng. Commun.* **144**: 113-158.
- Weiland, R. H., J. C. Dingman, D. B. Cronin and G. J. Browning (1998). Density and Viscosity of Some Partially Carbonated Aqueous Alkanolamine Solutions and Their Blends. *J. Chem. Eng. Data* **43**(3): 378-382.

Vita

Chukwuemeka (Chuck) I. Okoye was born on March 12, 1979 in Owerri, Nigeria to Vincent Chukwuemeka and Monica Enuma Okoye. He completed High School Education at Federal Government College, Enugu and enrolled at the University of Maryland, College Park for his undergraduate studies in Chemical Engineering in 1996. At Maryland, he participated in the cooperative education program for two semesters as an employee of DuPont Specialty Chemicals in Wilmington, Delaware and completed a summer internship with W.R.Grace in Columbia, Maryland. In addition, Chuck studied business within the IBM Total Quality program at the University of Maryland and was also active member of Iota Phi Theta, Inc., a national social service fraternity. Upon receiving his BSChE with honors in 2001, Chuck took a business analyst position with Accenture LLP in Reston, Virginia and worked there for two years before returning to school for graduate studies in Chemical Engineering at The University of Texas at Austin. He graduated May 2005 with an M.S.E. and has accepted a full-time employment offer with ExxonMobil Chemical Company in Baytown, Texas.

Permanent Address: 8 Ambling Way

Owings Mills, MD 21117

This thesis was typed by the author.